
# NAVAL POSTGRADUATE SCHOOL

**MONTEREY, CALIFORNIA**

# THESIS

**QUANTUM EFFICIENCY AS A FUNCTION OF TEMPERATURE IN METAL PHOTOCATHODES**

by

Abdullah Kara

June 2013

Thesis Co-Advisors: Richard L. Swent
John R. Harris

THIS PAGE INTENTIONALLY LEFT BLANK

# REPORT DOCUMENTATION PAGE

*Form Approved OMB No. 0704–0188*



| **1. AGENCY USE ONLY *(Leave blank)*** | **2. REPORT DATE** June 2013 | **3. REPORT TYPE AND DATES COVERED** Master's Thesis |
|---|---|---|

**4. TITLE AND SUBTITLE**
QUANTUM EFFICIENCY AS A FUNCTION OF TEMPERATURE IN METAL PHOTOCATHODES

**5. FUNDING NUMBERS**

**6. AUTHOR(S)** Abdullah Kara

**7. PERFORMING ORGANIZATION NAME(S) AND ADDRESS(ES)**
Naval Postgraduate School
Monterey, CA 93943–5000

**8. PERFORMING ORGANIZATION REPORT NUMBER**

**9. SPONSORING /MONITORING AGENCY NAME(S) AND ADDRESS(ES)**
N/A

**10. SPONSORING/MONITORING AGENCY REPORT NUMBER**

**11. SUPPLEMENTARY NOTES** The views expressed in this thesis are those of the author and do not reflect the official policy or position of the Department of Defense or the U.S. Government. IRB Protocol number ____N/A____.

**12a. DISTRIBUTION / AVAILABILITY STATEMENT**
Approved for public release;distribution is unlimited

**12b. DISTRIBUTION CODE**

**13. ABSTRACT (maximum 200 words)**

Photocathodes, in which light is used to extract electrons from materials by the photoelectric effect, are the principal electron sources for many linear accelerators and Free Electron Lasers (FELs). There is an increasing interest in the use of superconducting radiofrequency electron guns, which work at cryogenic temperatures, and therefore require photocathodes that work at cryogenic temperatures as well. The primary metric used to quantify photocathode performance is the cathode's Quantum Efficiency (QE), which is the ratio between the number of incoming laser photons and outgoing electrons. The objective of this thesis is to measure the QE of metal photocathodes as a function of temperature. To accomplish this, a photocathode test stand capable of varying the temperature of metal samples from 80 K to 400 K was developed, and copper and niobium samples were tested using it. The QE of copper was found to vary by a factor of more than four over this temperature range, while the QE of niobium showed only slight temperature dependence.

**14. SUBJECT TERMS** Photocathodes, Niobium, Cryogenic Temperature, Quantum Efficiency.

**15. NUMBER OF PAGES** 85

**16. PRICE CODE**

| **17. SECURITY CLASSIFICATION OF REPORT** | **18. SECURITY CLASSIFICATION OF THIS PAGE** | **19. SECURITY CLASSIFICATION OF ABSTRACT** | **20. LIMITATION OF ABSTRACT** |
|---|---|---|---|
| Unclassified | Unclassified | Unclassified | UU |

NSN 7540–01–280–5500

Standard Form 298 (Rev. 2–89)
Prescribed by ANSI Std. 239–18

THIS PAGE INTENTIONALLY LEFT BLANK

**Approved for public release;distribution is unlimited**

# QUANTUM EFFICIENCY AS A FUNCTION OF TEMPERATURE IN METAL PHOTOCATHODES

Abdullah Kara
Lieutenant Junior Grade, Turkish Navy
B.S., Turkish Naval Academy, 2007

Submitted in partial fulfillment of the
requirements for the degree of

**MASTER OF SCIENCE IN APPLIED PHYSICS**

from the

**NAVAL POSTGRADUATE SCHOOL**
**June 2013**

Author: Abdullah Kara

Approved by: Richard L. Swent, PhD
Thesis Co-Advisor

John R. Harris, PhD
Thesis Co-Advisor

Andres Larraza, PhD
Chair, Department of Physics

THIS PAGE INTENTIONALLY LEFT BLANK

# ABSTRACT

Photocathodes, in which light is used to extract electrons from materials by the photoelectric effect, are the principal electron sources for many linear accelerators and Free Electron Lasers (FELs). There is an increasing interest in the use of superconducting radiofrequency electron guns, which work at cryogenic temperatures, and therefore require photocathodes that work at cryogenic temperatures as well. The primary metric used to quantify photocathode performance is the cathode's Quantum Efficiency (QE), which is the ratio between the number of incoming laser photons and outgoing electrons. The objective of this thesis is to measure the QE of metal photocathodes as a function of temperature. To accomplish this, a photocathode test stand capable of varying the temperature of metal samples from 80 K to 400 K was developed, and copper and niobium samples were tested using it. The QE of copper was found to vary by a factor of more than four over this temperature range, while the QE of niobium showed only slight temperature dependence.

THIS PAGE INTENTIONALLY LEFT BLANK

# TABLE OF CONTENTS

# LIST OF FIGURES

# LIST OF TABLES

THIS PAGE INTENTIONALLY LEFT BLANK

# LIST OF ACRONYMS AND ABBREVIATIONS

| | |
|---|---|
| CW | Continuous Wave |
| DF | Deuterium Fluoride |
| DoD | Department of Defense |
| FCT | Fast Current Transformer |
| FEL | Free Electron Laser |
| GaAs | Gallium Arsenide |
| HEL | High Energy Laser |
| LINAC | Linear Accelerator |
| LN | Liquid Nitrogen |
| ONR | Office of Naval Research |
| QE | Quantum Efficiency |
| SCL | Space Charge Limit |
| SRF | Superconducting Radiofrequency |
| WSMR | White Sands Missile Range |

THIS PAGE INTENTIONALLY LEFT BLANK

# ACKNOWLEDGMENTS

I would first like to thank my patient and grace-filled wife, Neslihan, who endured my absence at home while I was doing my experiments at Sp044 for long periods. I would also like to thank my thesis advisors, Dr. Richard L. Swent and Dr. John R. Harris, who helped me with all their efforts whenever I needed them, even across great distances. In addition, I want to express my gratitude to Beam Physics Group members Wayne, Andrea, and Mark for their assistance in preparing the test stands and in conducting the experiments. Finally, I also want to say thank you to one more person, James Sears, who provided me with the niobium samples for free. If I have done a good job, you all must know that I accomplished it with your help. Thank you.

THIS PAGE INTENTIONALLY LEFT BLANK

# I. INTRODUCTION

## A. LASERS FOR THE NAVY

After the invention of the laser in 1960, the idea of using a laser as a weapon quickly became of interest to the U.S. defense establishment, which began investing in this technology [1]. In 1968, Ed Gerry achieved a 100-kW output with a gas dynamic carbon dioxide laser, further accelerating interest in laser weapons [2]. Different agencies pursued different technology approaches based on their own military requirements. For the Navy, interest in high energy laser (HEL) weapons was primarily driven by the need to defend surface warships, especially carriers and their escort ships, against incoming anti-ship missiles. Lasers were seen as a potential counter to this threat for several reasons.

- Since no ammunition is expended, the cost per engagement can be smaller with a laser than with other anti-missile systems.
- Many laser systems have the potential to be very compact.
- Laser weapons do not require the storage of explosive rounds, which can endanger the ship.
- Laser energy travels with the speed of the light, while a typical bullet travels with an initial speed of Mach 3.5.
- The range of the laser is defined by the horizon, while a bullet is limited by atmospheric drag and gravity.

The Navy's HEL program soon demonstrated the ability to successfully engage airborne targets with lasers. Much of this work was performed at the White Sands Missile Range (WSMR), where a facility for testing high-power lasers had been authorized by Congress in 1976 [3]. There, the SeaLite system, which used an MW-class Deuterium Fluoride (DF) laser, shot down a BQM-34 drone aircraft in 1986. Three years later, the system shot down a Talos missile simulating a supersonic cruise missile on a crossing trajectory at a tactically meaningful range. Nevertheless, the system was not ideally suited for shipboard applications due to its wavelength, which limited propagation through the

atmosphere. Additionally, it used toxic chemicals which were dangerous to the crew and required frequent replenishment [4].

In parallel with chemical laser development, a new concept called the Free Electron Laser (FEL) was suggested by J.M.J Madey in 1971 while he was at Stanford University [5]. This concept did not use a chemical medium to obtain laser light. Instead the new laser used a beam of free electrons. This concept provided several potential advantages for the Navy:

- FELs avoided use of toxic chemicals which introduce additional damage control and resupply problems for the warfighters.
- With no conventional lasing medium, the problem of waste heat extraction was greatly simplified, providing the potential for very high-power operation.
- Since it did not depend on quantum mechanical transitions between discrete energy status, as in other types of laser, it could be designed to operate at wavelengths that were favorable for energy transmission through the atmosphere [6].

Because of these features, the Navy believed that the FEL had significant potential as a laser weapon, and the Navy officially initiated its FEL program in 1997 [7].

According to the Office of Naval Research (ONR):

> The capability of having speed-of-light delivery for a wide range of missions and threats is a key element of future shipboard layered defense… This revolutionary technology allows for multiple payoffs for the warfighter. The ability to control the strength of the beam provides for graduated lethality, and the use of light vice an explosive munition, provides for lower per-engagement and life cycle costs. Not worrying about propulsion and working at the speed of light allows for precise engagement and the resulting low collateral damage. Speed-of-light engagement also allows for a rapid reaction to moving and/or swarming time critical targets [8].

Based on recent information, a new FEL weapon is envisioned for shipboard use within ten years [9].

## B. FREE ELECTRON LASERS

### 1. Components of an FEL

There are two types of FELs which are in most common use, the oscillator configuration and the amplifier configuration. Coherent operation (lasing) requires microbunching of the e-beam at the laser wavelength. Oscillators produce this microbunching by using an optical cavity to feed spontaneous radiation back into the undulator, while an amplifier uses an external source of light to generate the microbunching.

The main parts of a typical FEL, as envisioned for use by the Navy and shown in Figure 1, include an injector, a linear accelerator, an undulator, an optical cavity, and a beam dump.

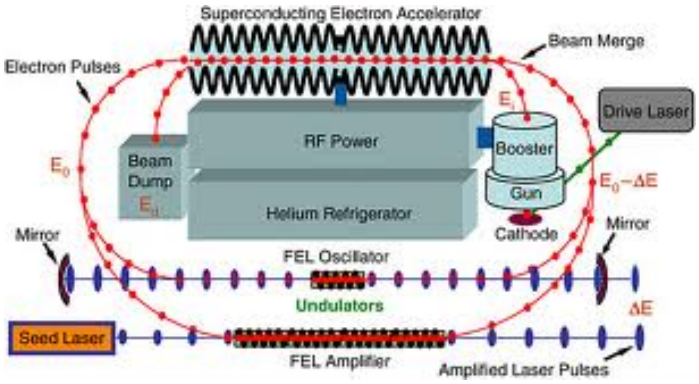


Figure 1. Schematic diagram of an FEL. From [8].

Electron beam production and initial acceleration occurs in the injector. This section contains a cathode (electron source) inside an electron gun and may also include a booster accelerator. Photocathodes are most commonly used as the electron source and will be described in the next sections.

In the FELs envisioned by the Navy, the electron beam will be transferred into a superconducting radiofrequency (SRF) linear accelerator (LINAC). This device contains several metal cavities in which high-power electromagnetic fields are used to accelerate electrons up to about 100 MeV.

After electrons are accelerated by the LINAC, they enter the undulator. The undulator contains a series of magnets which supply an alternating magnetic field that moves the electrons back and forth. This wiggling causes photon emission from the relativistic electrons.

The undulator is typically located within an optical cavity. In an oscillator-type FEL, the optical cavity comprises two mirrors located at the ends of the cavity. One of the mirrors is partially transmissive, while the other one is fully reflective. These mirrors provide the feedback needed for the FEL oscillator to start up from noise, while still allowing some of the optical power in the cavity to exit through the partially transmissive mirror and to be sent through the beam director and on to the target.

Amplifier-type FELs, on the other hand, use a seed laser instead of mirrors to produce gain.

Only a small fraction of the electron beam power will be converted to laser light. Recycling the rest of the electron beam energy will increase the FEL's overall efficiency. In order to achieve this, a large quantity of the electron beam power must be reclaimed. To do this, the electron beam exiting the undulator is directed by magnets to re-enter the accelerator. However, this time they will enter with a 180-degree phase shift. This phase shift causes them to release their energy to the RF field and slow down. After as much energy as possible is removed from the electron beam, it will be sent to the beam dump. The beam dump absorbs the remaining beam energy, in the process generating heat and x-rays, which requires that the beam dump be shielded and cooled.

## 2. How FELs Work

An FEL produces laser radiation using the energy from a relativistic beam of electrons. In FELs, electron beams are used as the lasing medium, while in conventional lasers, a gas, liquid, or solid is utilized for this purpose. This accounts for many of the differences between conventional lasers and FELs. For example, in conventional lasers waste heat must be extracted through the lasing

medium, while in an FEL the waste heat is removed from the lasing region at nearly the speed of light as a part of the electron beam. In addition, the lasing medium in a conventional laser limits it to specific wavelengths, while the FEL offers both “designability” (to select the band before the FEL is built) and “tunability” (to adjust the wavelength within that band after the FEL is built).

After the electrons are produced and accelerated to relativistic speeds, they are directed to enter the undulator. The undulator produces an alternating magnetic field which creates a strong Lorentz force that deflects the electron beam back and forth, causing the beam to radiate electromagnetic energy. Creating an optical field that interacts with the electron beam causes bunching of the electrons at the optical wavelength. The FEL wavelength is given by

$$\lambda_\ell = \frac{\lambda_u}{2\gamma^2}\left(1+\frac{K^2}{2}\right), \tag{1.1}$$

where $\lambda_\ell$ is the light wavelength, $\lambda_u$ is the undulator wavelength, and $\gamma$ is the Lorentz factor. The undulator parameter is given by $K = \frac{eB_{rms}\lambda_u}{2\pi mc^2}$, and depends on the magnetic field B, undulator period, electron charge e, speed of light c, and electron mass m [9].

Once the electrons have become microbunched at the optical wavelength, they are able to coherently radiate at that wavelength. The radiation power then scales with the square of the number of electrons, rather than with the number of electrons, as is the case for non-coherent (spontaneous) emission. The radiation process by which the electrons give up a significant fraction of their energy to the optical field is therefore more efficient, increasing the power in this field and therefore generating gain.

## C. SRF LINEAR ACCELERATORS

Radio frequency linear accelerators are widely used for acceleration of electron beams. These structures use high-frequency, high-power electromagnetic fields synchronized with the electron beam, which enables the

electrons to gain energy from the fields, allowing them to gain hundreds or thousands of MeV in some machines. It is from this energy that an FEL is able to generate laser light.

Traditional accelerators are made of copper and can work at room temperature, with cooling provided by water serving to remove heat deposited in the copper due to the electrical power loss. However, a new type of linear accelerator has been developed over the past few decades, which uses superconducting materials such as niobium instead of copper (Figure 2). These structures are very efficient due to their very low electrical losses and are well-suited to continuous wave (CW) operation. One disadvantage of these structures is that they must be operated at cryogenic temperatures in order to stay superconducting.

Despite this disadvantage, SRF linear accelerators are the structures of choice for future Navy FELs due to their very low electrical losses, which is essential to efficiently transfer energy from the decelerating beam to the accelerating beam in “energy-recovery linac” configurations such as the one shown in Figure 1.

Figure 2. Superconducting RF accelerating cavity. From [10].

## D. SRF RESEARCH AT THE NAVAL POSTGRADUATE SCHOOL (NPS)

With the increasing interest by the Navy in FELs as future weapon systems for shipboard use, the FEL research group at the NPS was expanded to include an experimental team, the NPS Beam Physics Laboratory, which is focused on the development of accelerator technologies needed for these systems. SRF technology has been of particular interest. This included SRF electron guns; while SRF accelerators have been in use for several decades, SRF electron guns are a relatively new development and not a mature technology.

The NPS Beam Physics Lab and its Boeing and Niowave collaborators were successful in building and testing the first purpose-built SRF electron gun in the United States. During initial testing, the cavity demonstrated acceptable beam parameters in terms of bunch charge and emittance, and it showed promise in progressing to the full design gradient [11]. Complete details of the design and commissioning of the gun were reported in [12]. Although some minor problems were encountered during the testing, such as the failure of the NbTi solenoid to superconduct, there were not any serious problems, such as severe multipacting or cavity quenching. By the end of the experiment the measured performance was found to be sufficient for NPS's planned FEL experiments in the infrared [12]. This successful demonstration of a new gun design only 24 months after concept represented a remarkably short development period compared to other electron gun projects.

## E. ELECTRON SOURCES FOR FELS

### 1. Electron Emission Process

Electrons are utilized to create the laser beam in FELs, but first we need to produce the electrons themselves. Under normal conditions, electrons stay inside solid matter because it is energetically favorable for them to do so. So to generate free electrons, we must either give them enough extra energy to overcome the energy barrier at the surface of the material, or we must change

the potential barrier. The amount of energy needed to extract electrons from the material is called the work function, and cathodes are classified according to how this energy is imparted:

"Thermionic emission" occurs when the cathode material is heated sufficiently so that some of the electrons inside the material gain enough kinetic energy to overcome the potential barrier. This type of emission happens in thermionic cathodes, which are widely used in microwave radar tubes.

"Secondary emission" occurs when a primary electron beam collides with a material and transfers some of its energy to the electrons in that material, giving these "secondary electrons" enough energy to overcome the potential barrier. Secondary emission plays an important role in the discharge process such as vacuum surface flashover and multipactor.

"Field emission" occurs when a very strong electric field is applied to the surface of the cathode material, causing the potential barrier at the surface to be distorted, reducing its effective width and allowing electrons to tunnel through it to the vacuum level and become free. Field emission cathodes are being studied by some researchers for use in FELs of the type being considered by the Navy.

An extreme case of modifying the potential barrier is the "plasma cathode." Plasma containing positive ions and electrons can be produced through various discharge processes, and by applying a strong electric field, the electrons can be extracted. Plasma cathodes are capable of producing very large currents, and therefore have potential use in high-power microwave sources. However, they are generally limited by the expansion of the plasma, an effect recently studied at NPS by A. Yilmaz, who conducted thesis research on a flashboard plasma cathode test stand [13].

### 2. Photocathodes

The focus of this thesis, however, is the photocathode, which is the most common source of electrons in FELs.

Photoemission, or the photoelectric effect, was first observed by Heinrich Hertz in 1887 and later explained by Albert Einstein in terms of quantum mechanics in 1921, for which he won the Nobel Prize [14], [15].

In photoemission, electrons are produced by light striking the cathode surface. According to photoelectric emission theory, if we want to remove electrons from the surface of a metal using this light, then the photons must impart an amount of energy to the electrons so that they exceed the work function. This is the minimum energy required to remove an electron from a solid's surface to a point directly outside the surface. In other words, this is the energy required to carry an electron from the Fermi level to the vacuum level. If the incident photon energy coming directly to the surface of the solid is less than the work function of the solid, then no electrons are emitted. If the incident photon energy is higher than the work function, the extra energy goes into kinetic energy of the freed electron.

The photoelectric work function is:

$$\Phi = h\nu \tag{1.2}$$

where "$h$" is the Planck's constant and "$\nu$" is the minimum (threshold) photon frequency required to produce photoelectrons. The work function depends on the type of cathode material used. Table 1 shows the work functions for typical photocathode materials used in FELs.

| | Cathode Material | Work Function (eV) |
|---|---|---|
| 1 | Magnesium (Mg) | 3.6 [17] |
| 2 | Lead (Pb) | 4.0 [16] |
| 3 | Niobium (Nb) | 4.38 [16] |
| 4 | Copper (Cu) | 4.6 [16] |
| 5 | CsBr:Cu (Coated) | ~ 2.5 [18] |
| 6 | CsBr:Nb (Coated) | ~ 2.5 [18] |

Table 1. Typical photocathodes.

Photocathodes are the most common electron sources used in FELs, because short-pulse lasers are available which turn the electron emission on and off very quickly, producing very short, high-quality electron pulses.

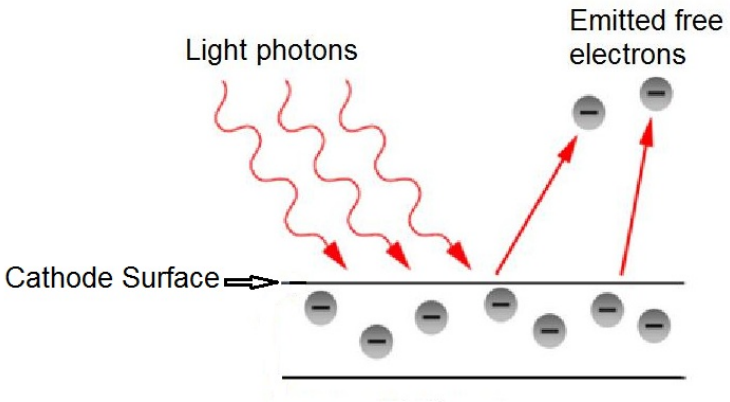


Figure 3. Photoemission.

After electrons are produced from the cathode, they need to be accelerated by a superconducting gun, for example, in order to make an electron beam. So both gun and cathode must be congruous with each other. For example, superconducting guns are operated at cold temperatures, in contrast to thermionic cathodes which work at high temperatures. Because of this, photocathodes are the most appropriate electron sources for this type of gun.

It is essential to define the effectiveness of a cathode sample used as a part of a vacuum electronic device; Quantum Efficiency (QE) is used as one such criterion. The QE is the ratio between the number of emitted electrons and the number of incident photons.

$$QE = \frac{\#electrons}{\#photons} \tag{1.3}$$

Different cathode samples have different QE values. Scientists desire to acquire robust, long lived, and high QE value cathodes. However, according to some studies [19], this situation does not seem to happen easily. Cathodes with

long lifetimes usually have low QEs, and vice versa; this trade-off between QE and long lifetime is shown in Figure 4.

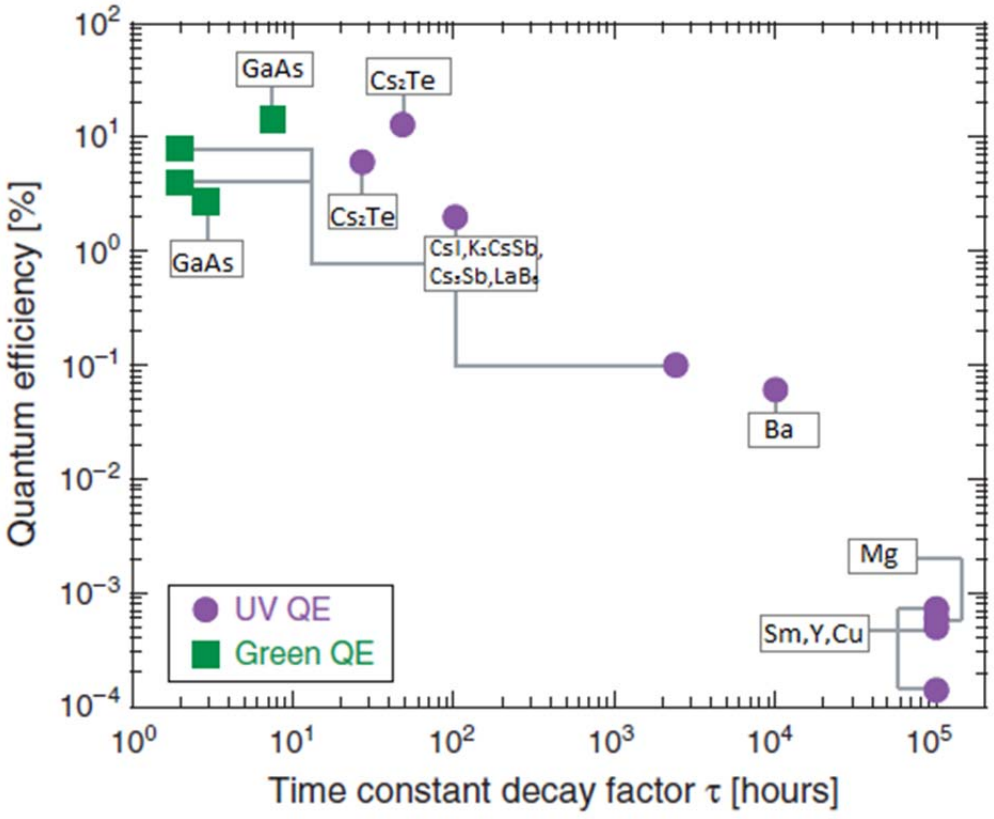


Figure 4. Photocathode QE versus lifetime of selected photocathodes under actual operating conditions. From [19].

## 3. Different Photocathode Types

Scientists have performed many experiments on photocathodes. They started their experiments with bare metals, such as copper, magnesium, etc. As time went by, more complicated materials were used because of the need for obtaining high QE values.

### *a. Metal Photocathodes*

These were the initial electron sources used by scientists as photocathodes. They are prompt, rugged, and have long lifetimes, but require higher intensity lasers as their QEs are on the order of 0.001 – 0.01% [20].

### *b. Dispenser Photocathodes*

By depositing other materials, such as a partial monolayer of cesium, on the surface of a metal photocathode, its work function can be reduced, and its QE can be increased. However, these layers are often fragile and require replenishment. In order to do this in situ, a compact configuration known as a dispenser photocathode has recently been introduced. This is an adaptation of the dispenser cathode geometry used in thermionic cathodes. The dispenser photocathode has a reservoir of low work function material which partially coats the cathode surface to improve its QE. Primarily these configurations were developed at the University of Maryland, with some testing done recently at NPS [21], [22].

### *c. Semiconductor Photocathodes*

Semiconductor photocathodes such as Gallium Arsenide (GaAs) require much lower-intensity drive lasers and can produce polarized electron bunches, but they generally require better vacuum conditions because they are more fragile [23]. Direct band-gap p-type semiconductor photocathodes, such as alkali antimonides and alkali tellurides, are the primary electron sources for many accelerators, and they are now in operation at the Thomas Jefferson National Accelerator Facility. They have high QE values on the order of 30% and are operable at longer wavelengths. However, they are chemically reactive, easily poisoned, and easily damaged by ion back bombardment [24].

# II. QE TEST STAND

## A. PHOTOCATHODE RESEARCH AT NPS

Previous cathode research projects have been performed at NPS with the aim of developing better electron sources than the ones currently used in accelerators and microwave sources. These projects investigated explosive emission [25], flashboard plasma [13], and cesium coated cathodes [21].

This research thesis is mainly focused on metal photocathode operation at both cryogenic and elevated temperatures. There has been much prior research on the measurement of QE of metal cathodes [26], [27], [28]. However, most of these experiments studied cathodes at or above room temperature, and we are not aware of any research on the dependence of photoelectron emission on the temperature of metal cathodes at cryogenic temperatures. As mentioned in the previous chapter, SRF electron guns work at very cold temperatures. In these systems, the cathode will stay in a cryogenic environment during the electron production process, so it is important to understand how the cathode will behave in this environment. In particular, we wanted to determine whether there is a temperature effect on the number of electrons produced for a given amount of incident light. To do this, we expose the cathode to light while it is at cryogenic and high temperature conditions, apply an electric field to extract the photoelectrons produced, and record the required data to calculate QE.

For a cathode material, we initially used copper, because it is abundant and cheap. Initial testing with copper was performed in a test stand without the ability to alter the cathode temperature, which allowed us to verify laser performance and test procedures. With the help of these results, a newly designed test stand and cathode stalk with the ability to control the cathode temperature were tested to verify operations. This was again done with a copper cathode first so as not to damage the main niobium sample. Later on, niobium,

which is more expensive and rare, was tested within the same test stand and under similar conditions.

The light source used in this research was a Continuum Minilite Nd:YAG laser, which produces a 5 ns long pulse of 266 nm UV light [29]. When the laser light is directed onto the cathode sample, the light excites the electrons over the surface potential barrier. A positive high voltage was applied to part of the vacuum system to behave as an anode. The electrons emitted from the cathode moved to the anode, causing a current flow along the cathode stalk towards the cathode. A Bergoz Fast Current Transformer (FCT-016–20:1-WB-H) was mounted around the cathode stalk for monitoring this electron flow on the cathode stalk, and therefore served as a measure of emitted current.

The components used to assemble the test stands, as well as the design and operation of the preliminary and the temperature-controlled test stands, are discussed in the remainder of this chapter.

## B. INFORMATION ABOUT THE EQUIPMENT USED

First of all to do this research, we needed to build a test stand which ultimately included nearly a dozen pieces of equipment, distributed among several main subsystems. This equipment is discussed here.

### 1. Laser

The laser is one of the key elements in our test stand. In this test stand, electrons are emitted by photoemission, requiring that we shine light onto the cathode's surface. In order to do this, we used a Continuum Minilite-II Nd:YAG laser. It is a Class 4 laser, which is the most dangerous laser type. Special safety goggles were worn to protect our eyes from the hazard of the laser light.


Figure 5. Continuum Minilite-II Nd:YAG laser.

### *a. Wavelength and Power*

The laser produces light in four different wavelengths between the ultraviolet (UV) and infrared (IR). These are 266, 355, 532, and 1064 nm. To select the best wavelength to shine on the cathode, we must find out the work function of the cathode materials. It is essential that the energy of the photons used exceeds this value to allow photoemission. As mentioned previously, the work function for niobium is 4.38 eV, and for Copper it is 4.6 eV. Of the wavelengths our laser can produce, only 266 nm satisfies this requirement, and so only 266 nm UV light is applied in our experiments [16].

The laser's power also varies with the wavelength. At the 266 nm wavelength, it can produce up to 40 mW.

### *b. Pulse Width*

Another principle specification of the laser is its pulse width. The Minilite produces a pulse of laser light which is 3 to 7 ns in width, depending on

the wavelength used. For 266 nm wavelength, its pulse width value is between 3–5 ns.

#### *c. Optical Elements*

In order to obtain pure UV light and control the laser power remotely, we mounted some optical elements, including some that were remote controlled, between the laser and the cathode. We placed a green light filter to block the green/visible light which was not fully converted to UV inside the laser. Another optical element was needed to balance the requirement for relatively low power at the cathode and relatively high power at our power meter. So, we inserted a 30% transmissive and 70% reflective beam splitter into the optical beamline. We also located a shutter blocking the laser beam and a remote-controlled polarizer to increase or decrease the laser power from outside the laser enclosure.

### 2. Laser Power Meter

We used a Coherent FieldMax-II TOP laser power and energy meter connected to a PM10 Air-Cooled Thermopile Sensor, which could detect wavelengths between 190 nm and 11000 nm. The power meter can detect laser powers between 10 μW and 30 kW with a thermopile sensor. However, during testing, we required that the laser power at the sensor was 5 mW because the sensor was not rated for lower power, and initial testing at lower incident power showed that the sensor's response was nonlinear outside its specified range.

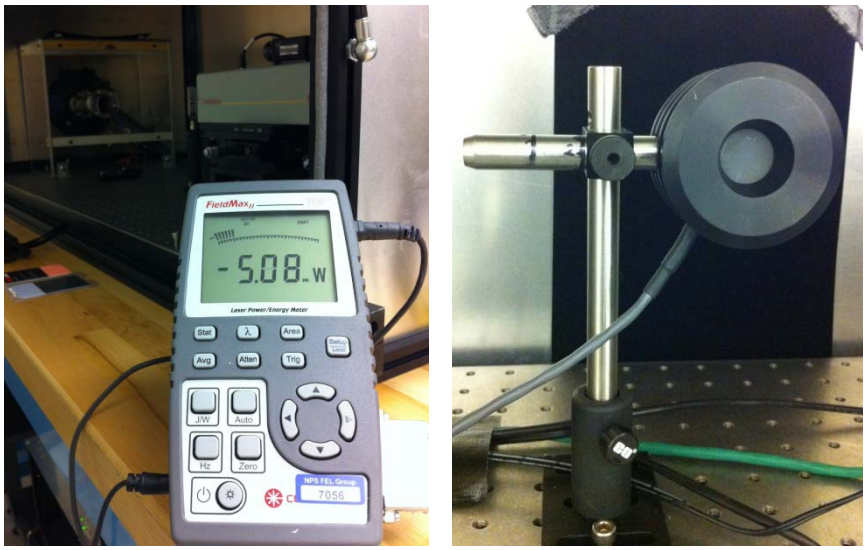


Figure 6. Laser power meter and sensor.

### 3. Cathode Stalk

As indicated, our aim is to measure QE under both cryogenic and high temperature conditions. To achieve this goal, we must cool and heat the cathode material; therefore, we designed and manufactured a new cathode stalk that holds the cathode and includes cooling and heating systems to add or remove heat from the cathode. Solid bulk copper was chosen for this purpose (Figure 7) because it is a very good conductor of heat.

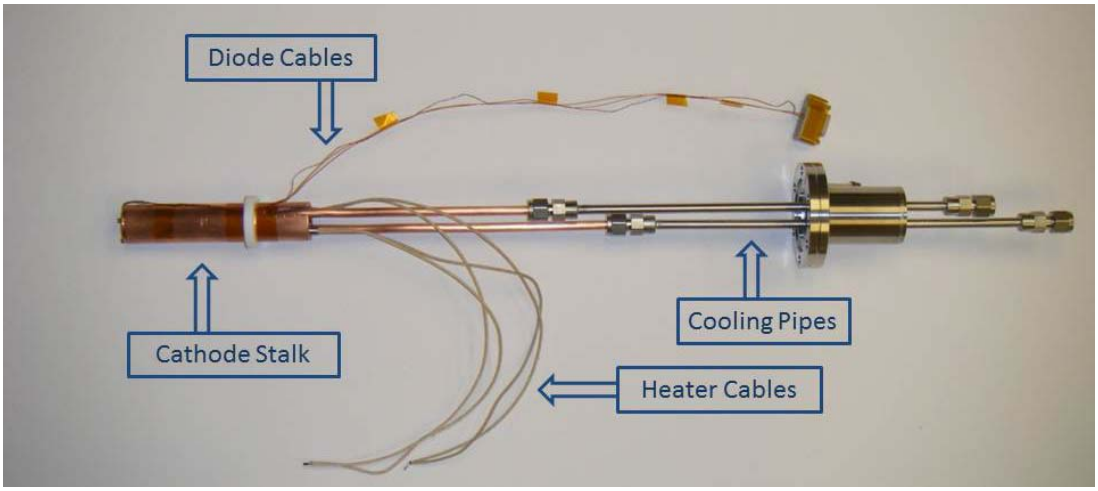


Figure 7. Cathode stalk with cooling and heating connections.

The cathode sample's diameter was 19 mm with a thickness of 3 mm. Before we placed the cathode samples in their locations on the cathode stalk, they were cleaned by using alcohol and lint free wipes.

For monitoring the cathode temperature, we used two temperature-sensing diodes of the type commonly used in cryogenic research. These were located at the very end of the cathode stalk, with one placed on either side of the cathode sample. The diode behind the cathode is a LakeShore DT-670-CU-HT, which withstands temperatures up to 500 K, and the diode in front of the cathode is a LakeShore DT-670-SD, which withstands temperatures up to 400 K. The diode behind the cathode is in a well and is pushed against the back of the cathode with a spring. The diode on the front is pushed against the cathode by the bent edge of the washer visible in Figure 8.

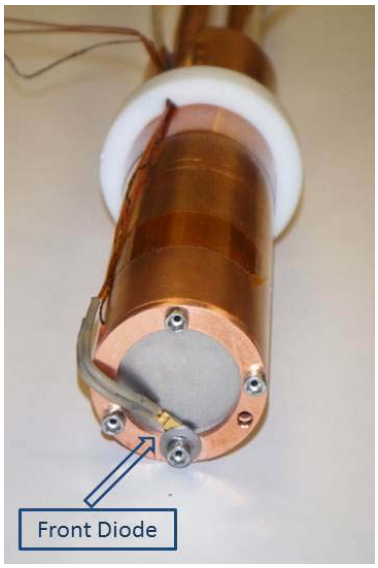


Figure 8. Cathode stalk holding niobium cathode sample and diodes.

### *a. Cathode Cooling System*

To take data from the test stand at cryogenic temperatures, we cooled the cathode to 80 K using the liquid nitrogen (LN) cathode cooling system previously built and tested by LT A. Baxter [30]. A fill-pot, shown in Figure 9, is used as a LN phase separator to provide more consistent LN flow to the cathode

stalk cooling coil by eliminating or reducing gas bubbles. This allows the system to cool faster and stay cold more efficiently. The fill-pot is connected directly to the dewar through a solenoid valve controlled by an AMI Model 186 Liquid Level Controller. There is a sensor inside the fill-pot to determine the level of the liquid.

Figure 9. Cathode cooling system connected to LN tank.

### *b. Cathode Heating System*

For heating the cathode up to 400 K, two cartridge heaters were placed into holes drilled in the cathode stalk. The heaters were connected to a variable autotransformer to supply variable voltage for heating the cathode. Both heaters and the autotransformer are shown in Figure 10.

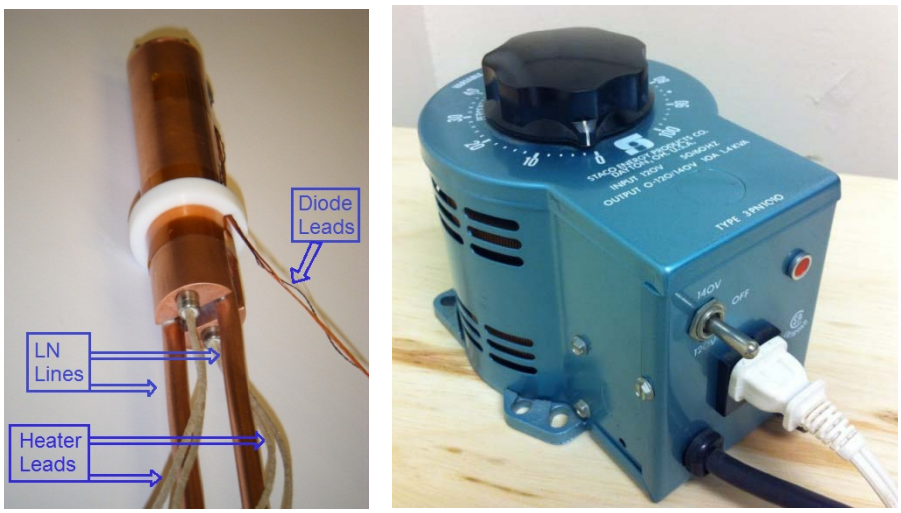


Figure 10. Cathode stalk with heaters and variable autotransformer.

## 4. Computer Software

We set up some useful software to control and monitor the heating and laser systems, which simplified and automated many of the required measurements.

### *a. Temperature Monitoring*

Two cryogenic diodes are located around the cathode to monitor the exact cathode temperature. Both diodes are connected to a computer via a LakeShore 218 temperature monitor, where we can see the increase and decrease of temperature. To do this easily, a LabView program written by Prof. Swent of the NPS Department of Physics, reads both temperature values and displays them on a chart, which makes it easier for us to recognize the general trend of the temperature, and saves this data to a file. The front panel display and representative data from this program are shown in Figure 11.

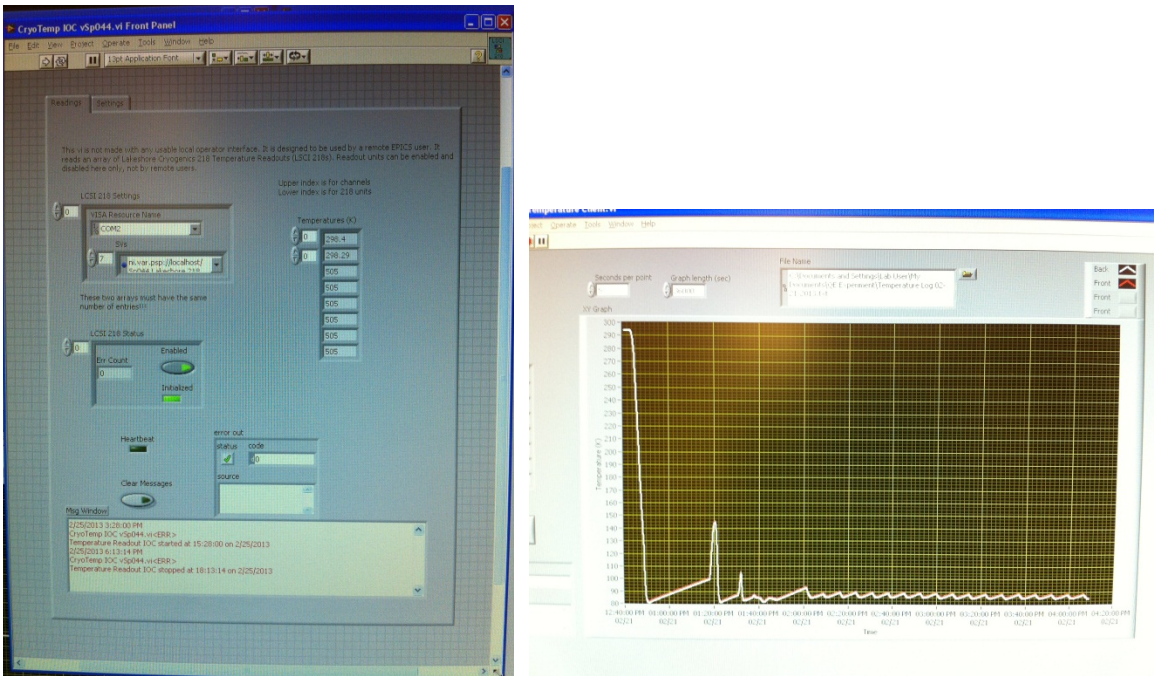


Figure 11. Temperature monitoring programs.

### *b. Automatic Laser Control*

We can control the laser beam by manually adjusting the laser power using a control lever on the laser head. However, for most of this work the laser system was inside an aluminum enclosure, which surrounded the high-voltage end of the test stand as well as the laser head, to protect us not only from the hazard of UV light but also from the high voltage (Figure 12).

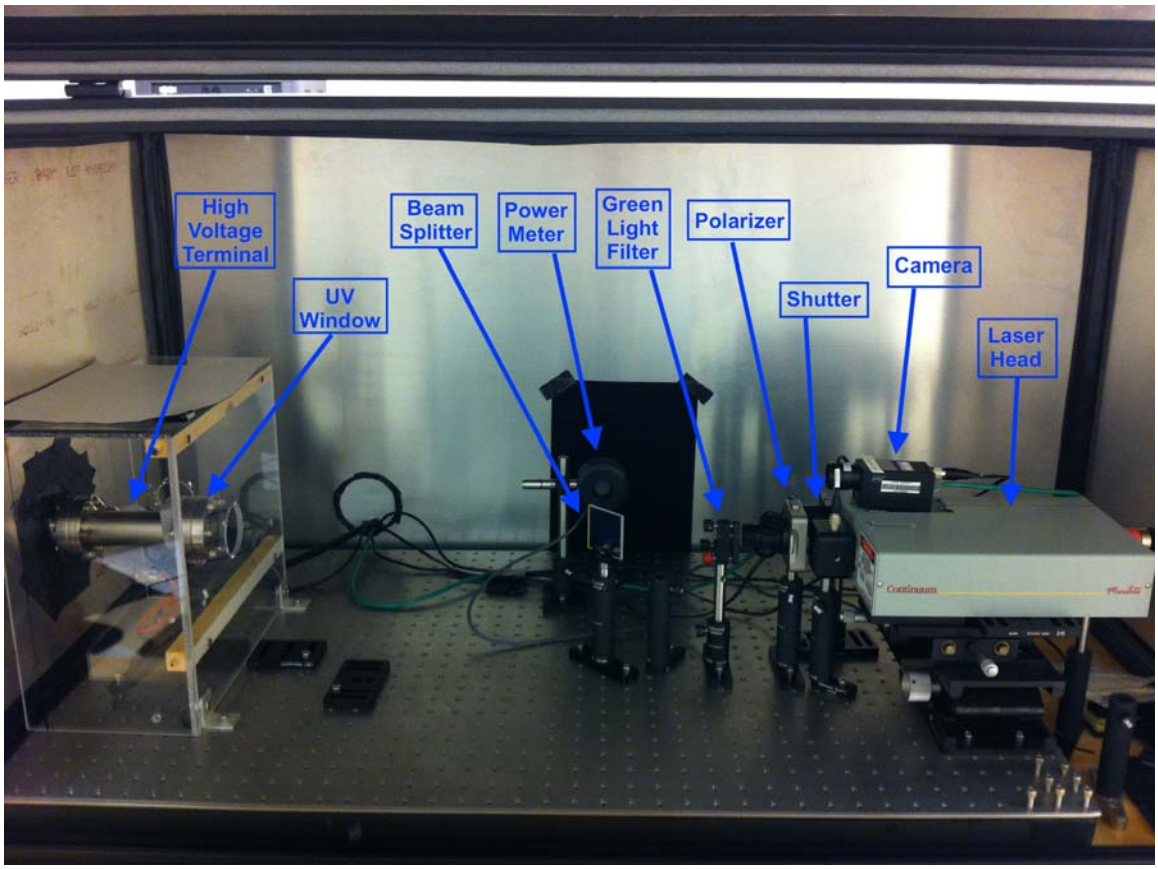


Figure 12. Laser system in aluminum enclosure.

To avoid having to open the enclosure frequently, we connected the laser beam control elements, such as the beam polarizer and shutter, to the same computer used for temperature logging, and another LabView program was written for controlling them remotely (Figure 13).

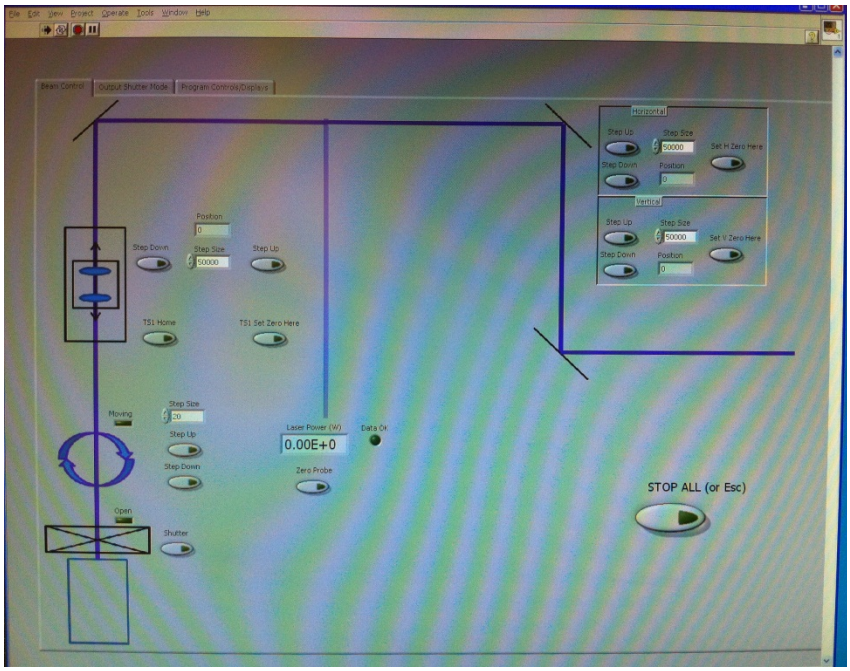


Figure 13. Laser remote control program.

## 5. Vacuum System

After the electrons leave from the cathode surface, they proceed towards the positively charged vacuum pipe, which serves as the anode. During this period they must move without hitting any molecules of air. Before we started assembling the test stand, every piece of the vacuum system was cleaned thoroughly with lint free napkins and alcohol to remove any contamination that might prevent the vacuum pressure from reaching satisfactory levels. We then connected two vacuum pumps onto the test set to remove the air.

The first pump was an Agilent model TPS-Compact 9698222 turbo pump, which was able to achieve a base pressure of about $10^{-6}$ Torr. An ion pump was added, and the vacuum level dropped down to $10^{-9}$ Torr (Figure 14). Vacuum pressure inside the test stands was a function of cathode temperature, and in practice the rate of cathode heating had to be limited to a level that did not cause the vacuum pressure to spike.


Figure 14. Agilent Technologies turbo and ion vacuum pump systems.

### 6. High Voltage Unit

In order to collect and direct the emitted electrons, there must be a positively charged piece called the anode. We connected a Glassman High Voltage unit which supplies a positive direct current (DC) voltage of up to10 kV to the vacuum spool piece in front of the cathode (Figure 15). A LeCroy high voltage probe was attached to the vacuum spool piece with the voltage to confirm the exact voltage value (Figure 16). Electrical insulation was provided by ceramic breaks.


Figure 15. Glassman high voltage unit.

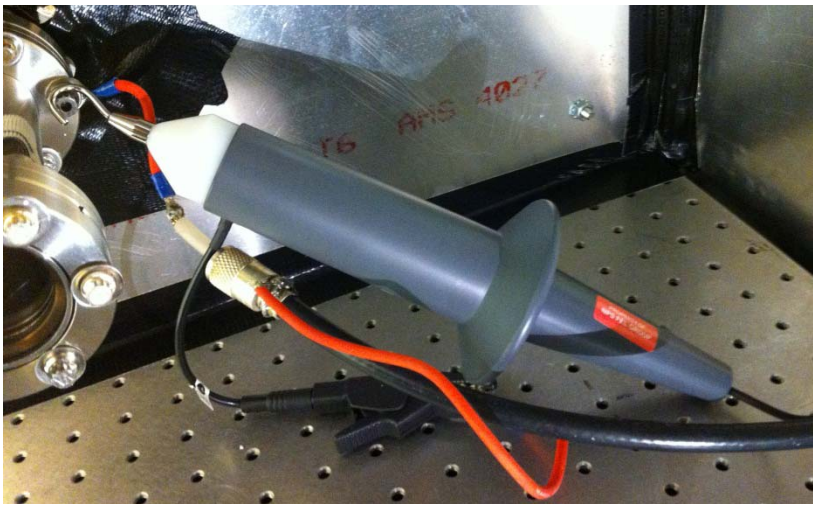

Figure 16. LeCroy high voltage probe.

## 7. Electron Beam Measurement

One of the most important requirements for this test stand is the ability to measure the electron beam current. This value, along with the laser power, was directly used for calculating the QE.

### *a. Bergoz Fast Current Transformer (FCT)*

This unit detects and measures the current due to the flow of electrons along the cathode stalk. It has a rise-time of 233 ps, which is sufficiently fast to provide time-resolved measurements of the photoelectron current produced by our 5 ns pulse width laser (Figure 17).

Because the process of photoemission from metals occurs much faster than this, the width of the laser pulse determines the width of the electron pulse. Ideally, we would like a diagnostic. For this we used a Bergoz Fast Current Transformer. The transformer's rise time is 233 ps, which is less than the light's pulse width. Therefore, it can measure the current accurately.

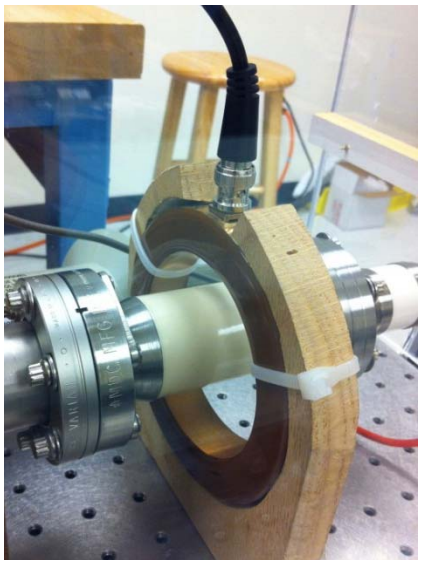

Figure 17. Bergoz Fast Current Transformer (FCT).

### *b. Oscilloscope*

The transformer was connected to an Agilent Technologies DSO7054B digital storage oscilloscope where we read and recorded the data. This oscilloscope also provides a capability to integrate the measured current to determine the amount of charge extracted from the cathode. This oscilloscope, along with a typical electron current and charge measurement, is shown in Figure 18.

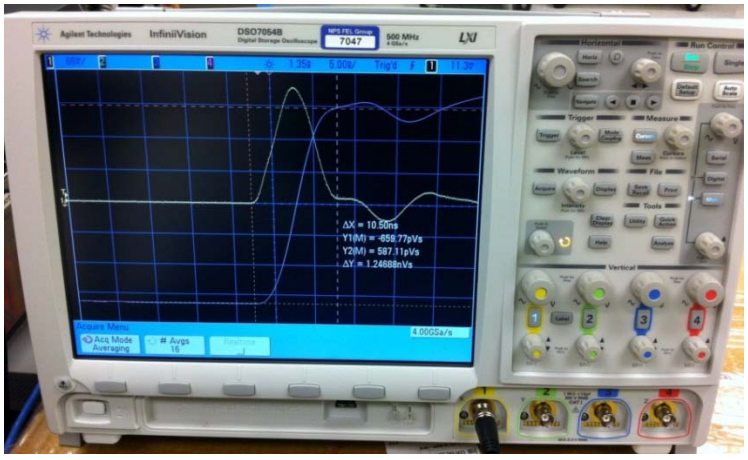


Figure 18. Agilent technologies oscilloscope.

## C. FIRST-GENERATION TEST STAND

At the beginning of this thesis research, a first-generation test stand was built which did not have the ability to control the cathode temperature or to test different cathode materials. Our aim with this test stand was to shake down the laser, high voltage supply, and associated equipment, and to gain experience using these systems to take photoemission measurements.

For the cathode in this test stand, we used a high-current vacuum feedthrough, which was already on hand. This feedthrough consisted of a solid copper rod mounted in a $2\frac{3}{4}$" conflat flange and was electrically isolated from the flange by a ceramic insulator (Figure 19). The copper rod had a flat surface, which was convenient for use as the emitting surface. However, the copper had been exposed to air and moisture for a long time. To remove its surface oxidation layer, the copper was dipped into a vinegar-salt mixture to clean the surface. After ten minutes a clear difference at the cathode's surface was seen, as shown in Figure 10.

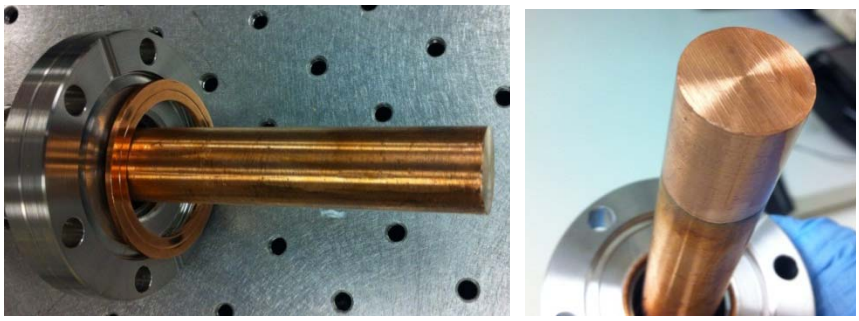

Figure 19. Cooper cathode before and after the vinegar cleaning.

After deciding on the cathode material, we started assembling the test set. Each component of the test set was cleaned meticulously with alcohol and lint free wipes to achieve a lower vacuum level, which was desired for getting good experimental results.

We should also mention another pump that was used in our initial test stand. It was a Varian Turbo-V 301-AG turbo pump, which was capable of reducing the vacuum inside the test stand down to about $10^{-7}$ Torr (Figure 20).

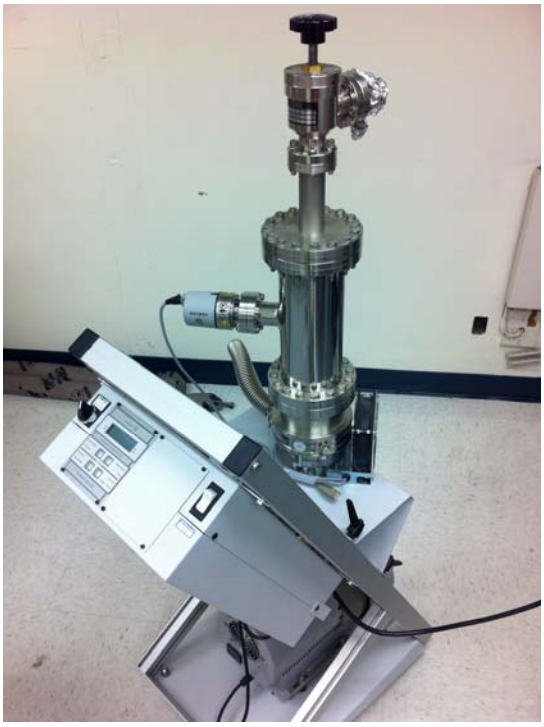

Figure 20. Varian Turbo-V 301-AG turbo pump.

High voltage from the Glassman power supply was applied to a vacuum spool piece to serve as an anode and attract the emitted electrons from the cathode. This spool was electrically isolated from the rest of the test stand with two ceramic breaks. One of these breaks was mounted coaxially with the cathode rod, and a Bergoz FCT was placed around it to measure the emitted current. The UV window where the laser beam enters the vacuum chamber was located at the end of the system near the vacuum pumping part. There was concern that the emitted electrons might move directly towards the UV window's inside surface and gather there, charging up the glass and causing a discharge leading to breakage or shattering. As a result, the window was placed as far downstream as possible and in a region of the test stand that was at the cathode,

rather than the anode, potential. The entire test stand was enclosed in a Plexiglas box to protect against the high voltage hazard (Figure 21).

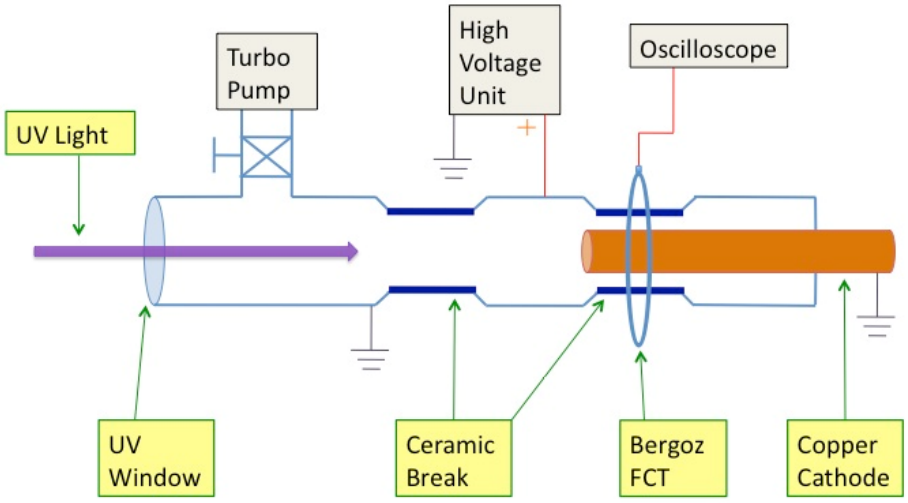


Figure 21. Schematic view of the first-generation test stand.

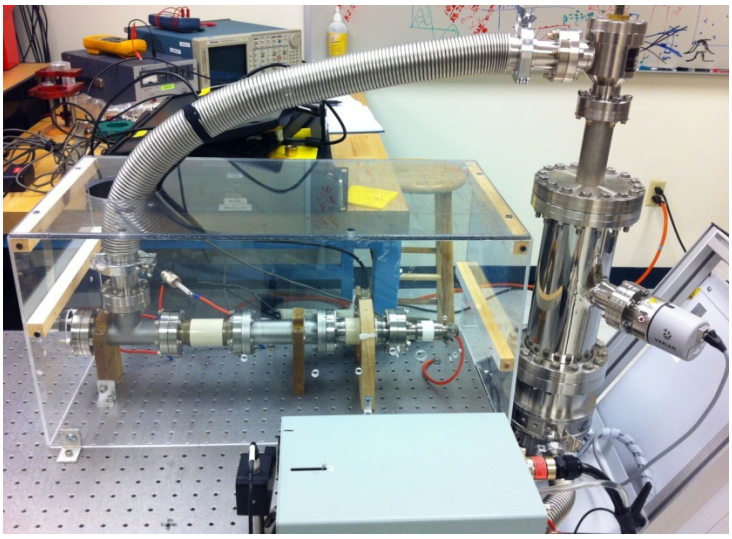

Figure 22. First-generation test stand.

Later we started using the test stand. At first we gained experience on using, controlling, and adjusting the laser beam. When we achieved a certain level of expertise with this, we pumped out the air from the chamber, applied high voltage, made the connection to the oscilloscope, and directed the laser onto the

copper cathode, producing our first photoelectrons. Our initial electron beam measurement taken on a Tektronix TDS 714L oscilloscope is shown in Figure 23.

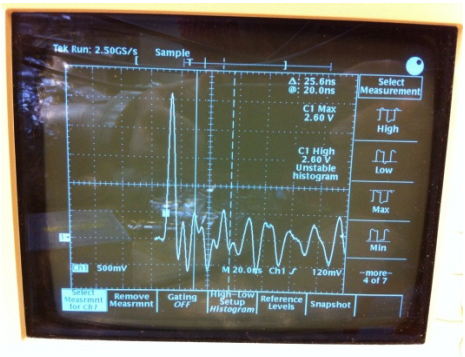


Figure 23. First measurement of electron emission from the cathode.

As expected, we observed that the electron current detected by the Bergoz FCT depended primarily on laser power for low laser power values. Electron current flow from a photocathode can be expressed by

$$I = \frac{\lambda P}{0.124} QE \quad , \tag{3.1}$$

where $I$ is the electron current (in mA), $\lambda$ is the laser wavelength (in nm), $P$ is the applied laser power (in mW), and $QE$ is the quantum efficiency (in percent) [29]. As we see from the equation, the laser power (P) and electron current are proportional to each other; they increase or decrease together linearly to hold the QE constant.

However, over a certain laser power level, the increase in current for a given increase in laser power ($\frac{dI}{dP}$) will decrease. This is not due to a change in QE, but rather due to space charge, an accumulation of charge in front of the cathode which serves to shield the cathode from the electric field produced by the anode and, therefore, to prevent the emission of additional electrons. Figure 24 shows experimental data obtained with the preliminary test stand. This data, plotted as peak current vs. laser power incident on the cathode for 20 different

voltage values from 0.5 kV to 20 kV, clearly shows both linear (emission-limited) region and the nonlinear (space-charge limited) regions.

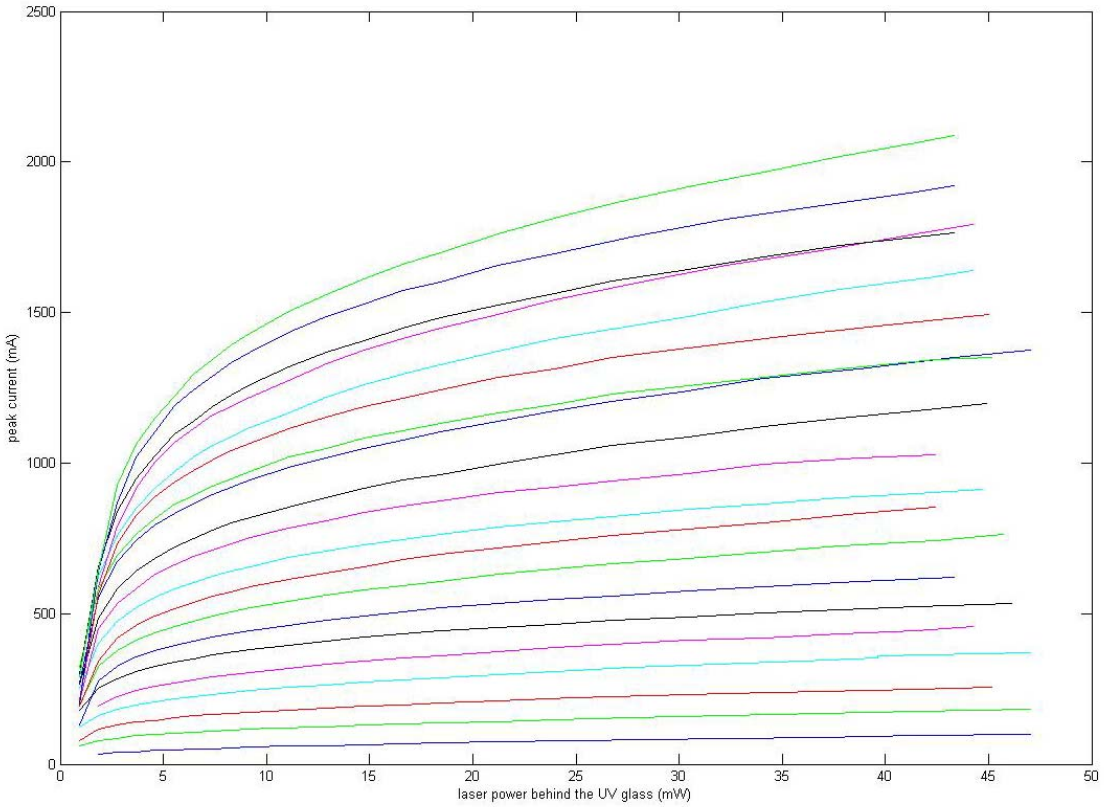


Figure 24. Laser power vs. peak current at 20 different voltages.

This data shows that the “space-charge limited” (SCL) regime started when the laser power reached around 5 mW. Because the objective of this project was to measure QE, it was essential to stay below the value at which the current was limited by space charge. And while the space-charge limited current depends on geometry, the temperature-controlled test stand was designed with a similar geometry, and therefore we expected to see similar behavior

After having gained experience with these issues, we were ready to start assembling our new cryogenic test stand.

## D. THE TEMPERATURE-CONTROLLED TEST STAND

We were now ready to initiate our new test stand and obtain new results. This time our goal was to include all the instruments which were not used on the previous test stand. In particular, our goal was also to add the ability to heat or cool the cathode.

In addition to incorporating the components discussed previously, the temperature-controlled test stand used larger-diameter vacuum pipes, providing improved pumping capacity. All the vacuum pieces were cleaned with alcohol and lint free wipes before assembly. The cathode stalk was the first part, which was located inside the vacuum chamber. Later, electrical connections for the temperature measuring diodes and heaters were made, and next the turbo and ion pumps were attached. The high voltage unit was attached directly to the front most vacuum element. Then, the cathode cooling system was connected to the whole test stand. Finally, an aluminum enclosure box protecting us from the high voltage and laser hazards was placed around the test stand.

Before we started conducting the experiment, we turned on the vacuum pumps. Initially the turbo pump was operated until the vacuum level inside the chamber dropped $10^{-6}$ Torr. Then, we turned on the ion pump to reduce the level more. Before we started taking data from the test stand, the vacuum level reached $10^{-7}$ - $10^{-8}$ Torr at room temperature conditions.

A schematic of the assembled test stand is shown in Figure 25, and a photograph of the test stand's control station is shown in Figure 26.

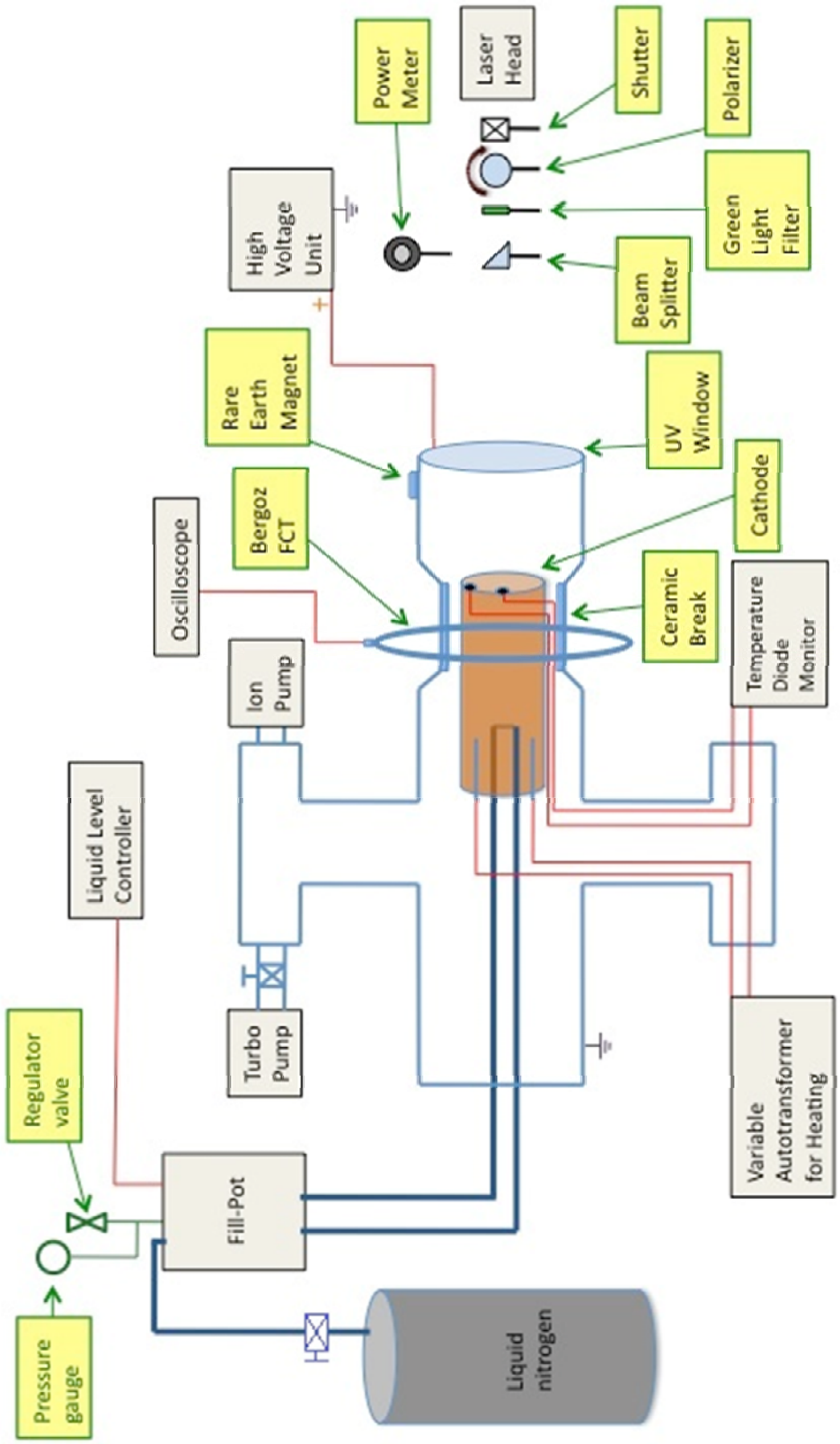


Figure 25. Schematic diagram of the temperature-controlled test stand.

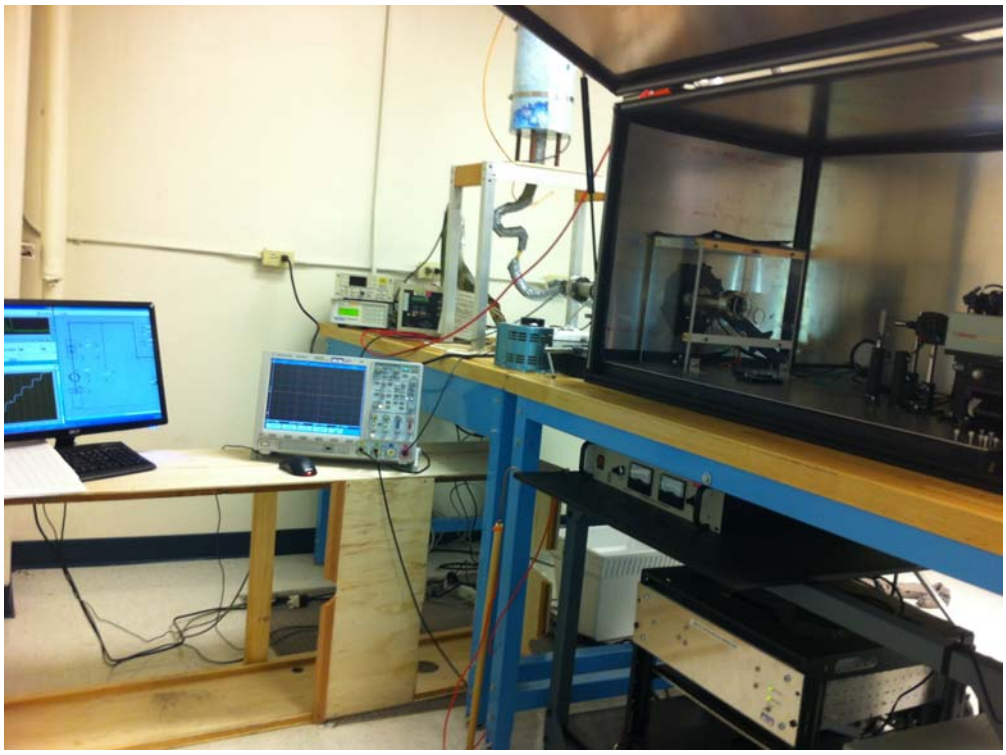

Figure 26. Temperature-controlled test stand.

When we finished building the test stand, we were ready to shine the laser on the cathode and make photoelectrons. This time, however, we also got the cooling and heating systems ready. For initial testing, a copper cathode sample had been inserted into the cathode stalk. We illuminated the cathode with the laser and observed the electron beam current on the oscilloscope, producing the oscilloscope traces of beam current vs. time. We were now curious to see whether there was a significant variation in the beam current when we changed the cathode temperature.

At first the cathode was heated gradually up to 400 K by applying current to the heaters with the variable autotransformer. We observed a significant increase in the beam current displayed on the oscilloscope screen. Next, we cooled the cathode down to 80 K by using LN. It was seen that there was also a significant reduction in the beam current compared to the signal seen at room temperature. These changes were much greater than we had expected. Thus, this scene upgraded our enthusiasm for achieving better results.

# III. HOW THE QE EXPERIMENT WAS CONDUCTED

## A. UV WINDOW TRANSMISSION LOSS CALCULATION

As expressed in Chapter I, we used UV laser light where the wavelength is 266 nm because of the work function of the copper and niobium. We mounted a UV window in front of the cathode stalk on the vacuum chamber, where the laser light entered. For actual calculations, we had to determine the most accurate laser power inside the vacuum chamber, and this required measuring the UV glass transmission loss.

A basic test stand was designed and utilized for this purpose. Our aims were to define the laser power just before and after the UV window and to calculate the transmission ratio. The laser light and UV window were aligned on the same plane.

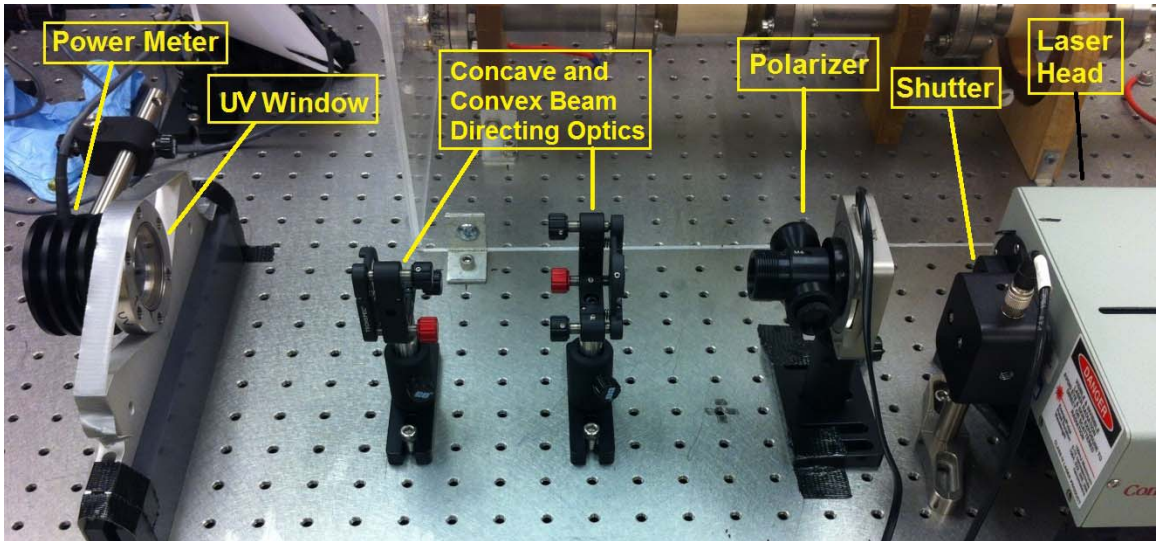


Figure 27. UV window transmission loss test stand.

This calibration process was conducted in two steps. In the first step the power meter was placed just in front of the UV window, and the laser power was measured and recorded. In the second step the laser power meter was placed immediately behind the UV window and the laser power was measured and

recorded. These values were used to find the fraction of laser power which was not transmitted through the window,

$$NT = \frac{P_2 - P_1}{P_1}, \tag{3.1}$$

where $P_1$ is the power upstream of the window, and $P_2$ is the power downstream from the window. Finally we used equation 3.2 to obtain the transmission coefficient "T."

$$T = 1 - NT \tag{3.2}$$

This measurement was repeated 19 times, with the power meter reversed between each measurement. Our average transmission coefficient found in this way was 0.922 ± 0.00.

## B. SPACE CHARGE LIMITED (SCL) REGIME IN TEMPERATURE-CONTROLLED TEST STAND

Achieving accurate QE results requires operating below the SCL. The SCL current depends on the geometry of the system and on the anode-cathode voltage, not on the cathode material.

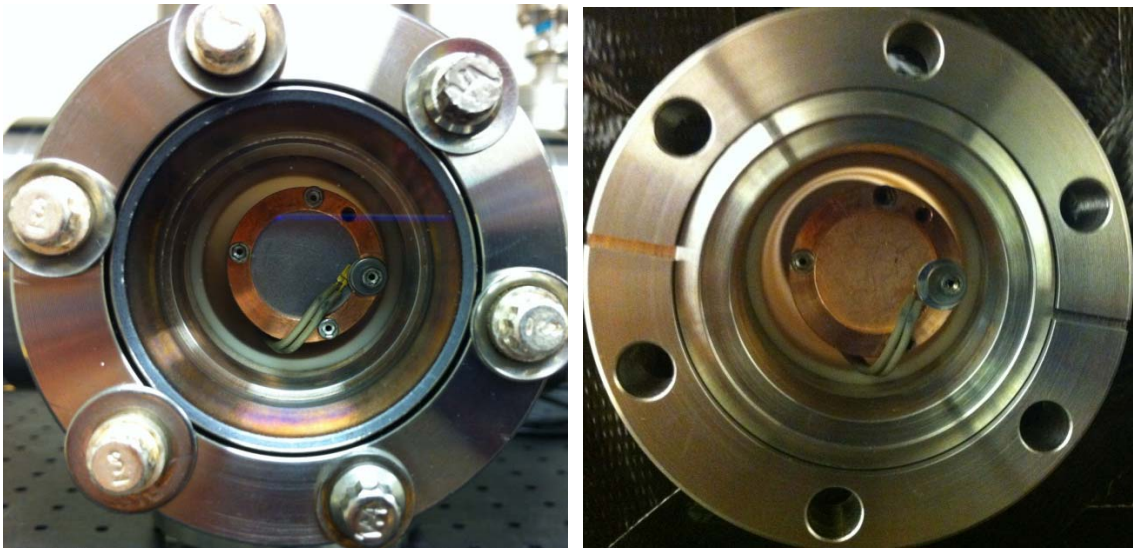

Figure 28. Niobium and copper cathodes in their locations on cathode stalk, respectively.

The geometry and the voltage used (10 kV) in the temperature-controlled test stand were very similar to those used on the first-generation test stand, so we expected to see the onset of space charge at about the same laser power, but repeated the measurement, giving the data shown in Figure 29, to verify this. As before, we gathered data at several different voltage values.

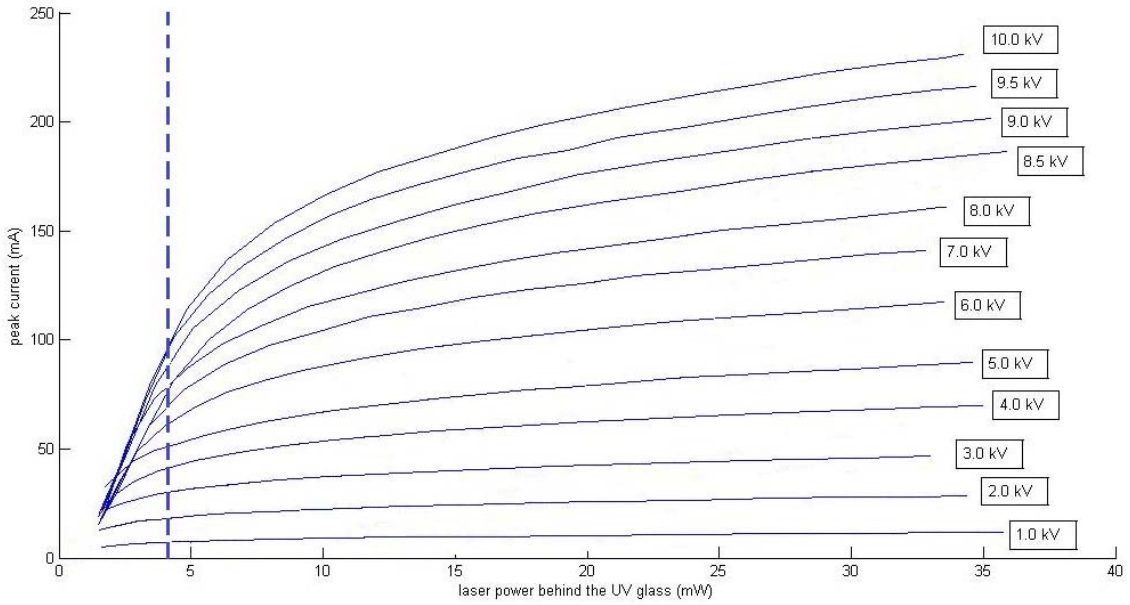


Figure 29. Laser power vs. Peak current for Nb SCL regime.

These results showed that for the planned operating voltage at 10 kV, SCL behavior started around 4 mW. This effectively set the upper limit on the amount of laser power that could be used in this experiment.

## C. QE MEASUREMENTS ON TEMPERATURE-CONTROLLED TEST STAND

The requirement to stay below 4 mW on the cathode and accurately measure the laser power applied to the cathode presented a problem for us. Our power meter could detect laser power values between 5 mW and 10 W; outside that range its response was nonlinear. So, it was difficult to detect the precise

laser power value on the cathode by placing the power meter just in front of the cathode for small values less than 5 mW.

To solve this problem, a 30T/70R beam splitter (which meant that 30 % of the laser light was transmitted and 70 % reflected) was placed between the laser head and cathode plane as shown in Figures 12 and 25. The power meter was stationed in the reflected beam direction. With the help of this small optical piece, we were able to measure the laser power more accurately. In this situation, our laser power was high enough for accurate measurement on the reflected side, and low enough on the transmitted side to stay below the SCL regime.

We could only measure the laser power on the reflected partition. To convert from this value to the laser power on the transmitted side, we multiplied the measured laser power by 0.4285, which was obtained by dividing the two nominal ratios for the beam splitter, which were 0.3 for transmission and 0.7 for reflection.

We completed our pre-requisite measurements, and we were ready to start taking data on the temperature controlled test stand. We prepared all the capabilities to control the laser while the enclosure box was closed. This was essential to protect ourselves from the possible hazard of high voltage and class-4 laser light. Every time before we started shining the laser, we allowed it at least 30 minutes to stabilize.

We used an averaged measuring mode to get a more stable laser power value. To do this, we set the power detection program's sample size to 600 so that it gathered 600 laser shots and displayed the power averaged over these shots, which took one minute. We recorded this value as our laser power for each experiment. The laser spot diameter on the cathode was 3.16 mm in these experiments.

It is also important to note the location of the laser spot on the cathode. The location and size of the spot on the cathode presents a possible source of error. If the spot is too big and too far off center, part of the laser might touch the

diode mount or the sample retaining ring, producing electrons from these materials and effectively “contaminating” the measurement. Also, if the spot is too big, it will sample regimes on the cathode surface which have different surface electric fields, and therefore, different SCLs. This could allow some regimes of the cathode to be SCL while others were emission-limited, altering the behavior of the system.

On the other hand, if the spot size were too small, the local photon flux density would be very high, possibly causing the system to reach SCL operation at lower total power levels. The actual spot size used represented a compromise between these extremes, and the spot location on the cathode was adjusted to avoid, as much as possible, both the cathode retaining ring and the diode mount. Additionally, from the measurements of the current vs. laser power, shown in Figure 29, we empirically found the value of laser power below which we could operate before the onset of space charge limited operation, thus avoiding the need to rely on simulations or even educated guesses to avoid this region [31].

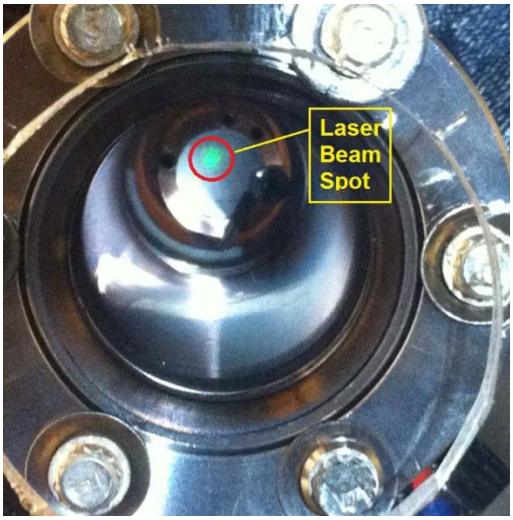


Figure 30. Laser beam spot on Nb cathode.

### 1. Cooling the Cathode Down to Cryogenic Temperatures

We started conducting our experiment initially by cooling the cathode. We used the cathode cooling system described in Chapter II [30]. Liquid nitrogen was our main source for achieving the cryogenic temperatures.

It usually took only ten minutes to reach 80 K. We held the temperature constant with the help of the cooling system without spending too much nitrogen. We ran all the software for recording the temperatures. The temperature monitoring program recorded the temperatures every five seconds from the diodes mounted around the cathode material. Number one and number two on the temperature monitor represented the temperatures for the diodes placed in the recess behind the cathode and on the emitting face of the cathode, respectively (Figure 31). There was almost no temperature difference between the two diodes; at 80 K the difference reached its maximum value of 1 K (Figure 31). However, while we were heating the cathode, the gap closed between the temperatures indicated by the two diodes. For our measurements, we accepted the first diodes value as temperature criteria.

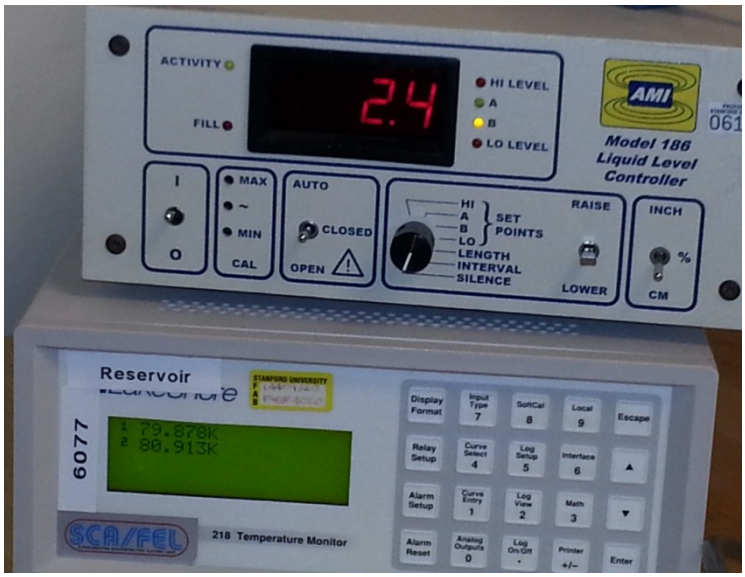


Figure 31. Temperature monitor at 80 K and Liquid level controller.

### 2. Creating a Stable Wave on the Oscilloscope

Initially the high voltage unit attached to the anode was turned on and set to 10 kV. When we produce free photoelectrons and remove them from the cathode's surface, then there must be an electron flow on the cathode stalk from the ground towards the cathode itself to maintain charge neutrality of the stalk. We aimed to detect this flow by placing a Bergoz FCT around the stalk. The FCT was connected to the oscilloscope's first channel, and a trigger signal from the laser was connected to the oscilloscope's second channel. By doing this, we set the scope to trigger on the laser's trigger signal, which gave a reliable display of the FCT signal even when it was small. We used the oscilloscope's averaging mode to acquire a more stable waveform on the screen. For this purpose, we set the oscilloscope to acquire 16 samples for averaging to display a more stable waveform.

### 3. Data Derived from the Test Stand

There were several quantities that we had to observe and record during the experiment process. Each of them needed to be taken carefully. We were dealing with very small amounts, and the tiny changes could produce huge effects on the ultimate result. So, we waited enough time with patience to derive the best results that we could reach.

Here are the variables recorded during the experiment.

#### *a. Cathode's Instant Temperature*

We always recorded this value by hand in the logbook. Furthermore, it was also logged in a file on the computer automatically by the software. It was essential for us to see the temperature changes on the cathode, because this was our primary variable.

### *b. Vacuum Level of the Cathode's Environment*

Before conducting the main experiment, we ran both ion and turbo pumps to remove as much of the air from inside the vacuum chamber as possible.

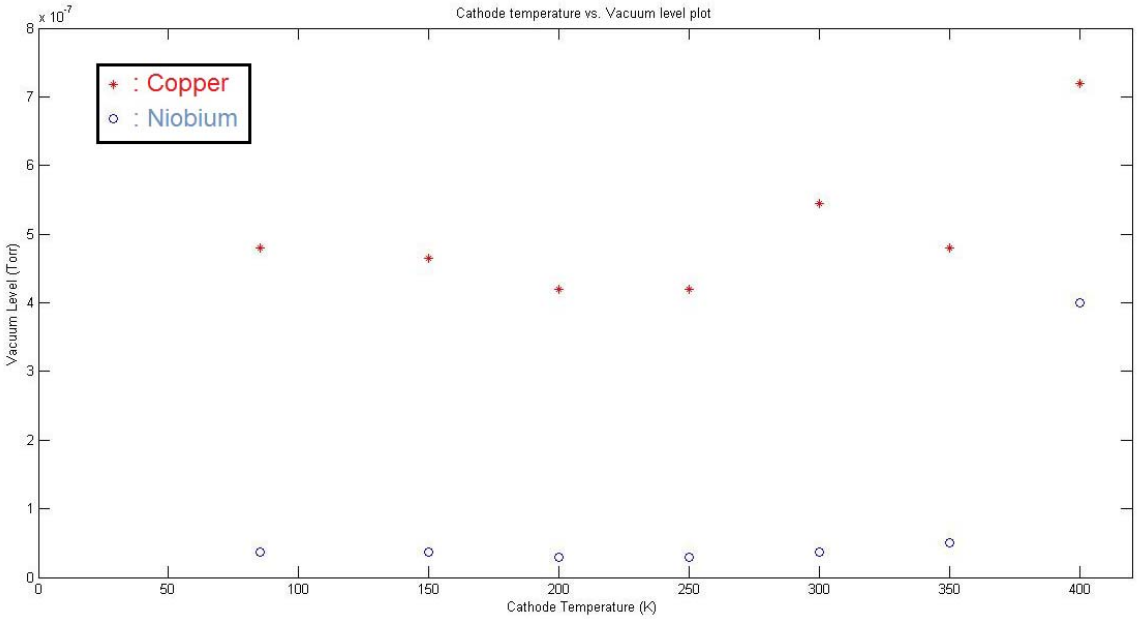


Figure 32. Cathode temperature vs. vacuum level.

The pressure inside the vacuum chamber depends on a number of features, including the cleanliness and the history of the test stand. Although all test stand pieces were cleaned carefully one by one, during the assembly period they might be exposed to lint and dust from the environment. Moreover, the test stand's usage cycle and how long the system components have been under vacuum could affect the vacuum level of the test stand.

But, in our experiment, the temperature of the cathode or the temperature of the vacuum chamber assumed the most significant role in determining the vacuum level. We ran across and observed this situation while we were conducting warm-up experiments with the copper cathode. While we were testing the cathode temperature increase, we went up too quickly by

applying a high percentage of current with the autotransformer. The beam current level on the oscilloscope increased, and the vacuum pressure increased at the same time with the same speed. At that time, we recognized a sudden blue light from the test stand, and the high voltage level which was normally 10 kV dropped to 0 V, indicating that a self-sustaining discharge had formed in the “vacuum” which was now filled with low-pressure gas desorbed from inside the heated test stand.

We turned all the systems off, discharged the test stand and opened the aluminum enclosure carefully. When we looked at the cathode’s surface, we saw that there was a discolored spot due to the discharge (Figure 33).

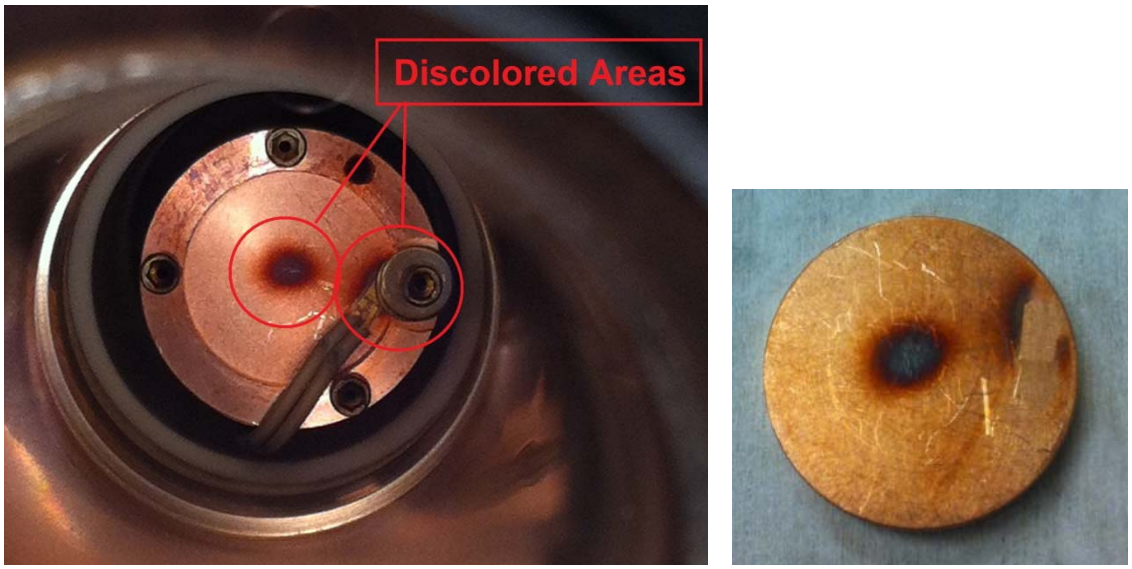


Figure 33. Discolored areas on the cooper cathode due to the discharge.

After that experience, we were more careful to increase the temperature of the cathode slowly in order to prevent a situation like this one in future experiments. We removed the damaged cathode and installed a brand new copper cathode for the future experiments.

We thought that the variation on the vacuum level inside the chamber could affect the electron production, and so it was recorded by hand during our experiments; except at high temperatures, there was very little change in vacuum pressure with cathode temperature during the actual experiments presented here (Figure 32).

### *c. Averaged Laser Power*

Laser power was the first key quantity, as it was used directly in the QE calculations as the denominator to calculate the number of photons inside the laser light beam. This value was important. Because of that, we spent most of our time trying to achieve a stable laser power value on the power meter program. It was recorded by hand, as well.

### *d. Charge Per Pulse*

The charge per pulse was the second key quantity in the experiment, because it gave us the number of emitted photoelectrons, and we used it as the numerator in the QE calculation. An intelligent tool inside the oscilloscope helped us to calculate the area. As is known, the area under a current vs. time graph gives us the amount of charge (Equation 3.3).

$$Q = \int I(t)\,dt \tag{3.3}$$

We defined the left and right boundaries of the pulse by using vertical lines; the tool integrated the area under the curve between the two of them and displayed the result. Then we recorded it by hand. Actually, the signal recorded on the oscilloscope is the voltage produced by the Bergoz FCT. This is proportional to the current passing through the FCT.

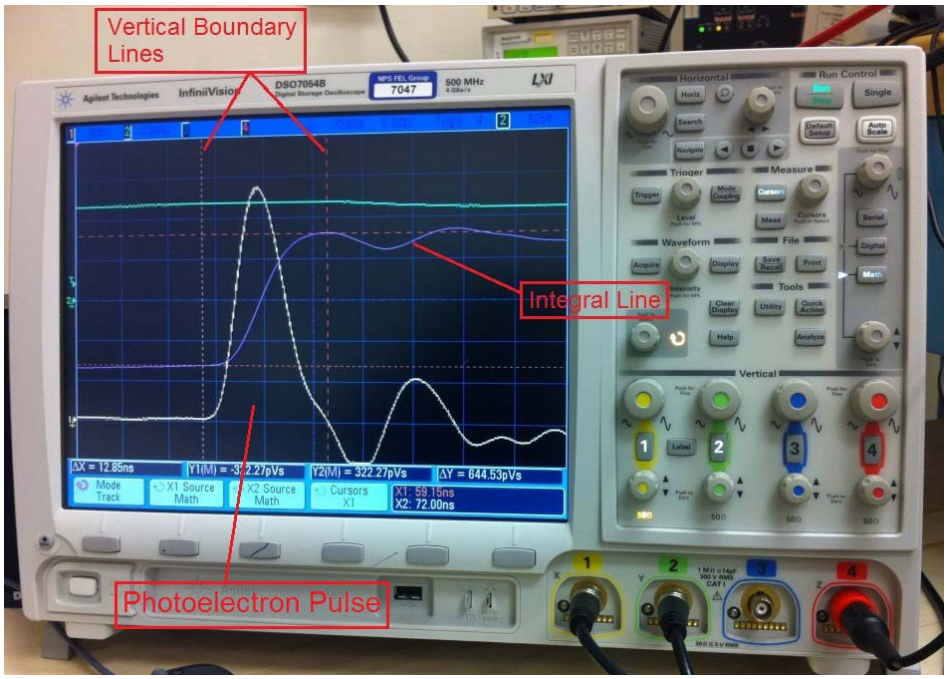


Figure 34. Photoelectron pulse on the screen with vertical boundaries.

### *e. The Peak Voltage Value of the Photoelectron Pulse on the Oscilloscope*

The peak voltage value was in a supporting role at the time of this experiment. However, during the SCL regime process, it was in the leading role. Here, we used this value as confirmation of whether we went beyond the SCL regime or not while we were conducting the experiment.

## 4. Heating the Cathode up to 400K

We did not heat the cathode suddenly to 400 K, but rather increased the temperature in 50 K increments (Figure 35). It was important for us to detect the QE values while the temperature was increasing up to 400 K to observe the behavior of the cathode sample. Whenever we reached the next data-collection temperature level, it was almost stable during the data collection process.


Figure 35. Image of temperature rise on computer software.

## D. PROCESSING THE RAW DATA

We collected enough required data from the test stand. However, they were not useful for calculating the QE until we processed them. At this time, we had to convert them to the number of electrons and protons.

### 1. Photon Number Calculation

We knew the laser wavelength and measured the laser power, which allowed us to determine the number of photons. Equation 4.1 gives us the amount of one photon's energy - $E$

$$E = \frac{hc}{\lambda}, \tag{4.1}$$

where $h$ is the Planck's constant, $c$ is the speed of light, and $\lambda$ is the photon's wavelength. The number of photons delivered in a single cycle (Figure 36) is related to the average laser power by

$$\#\ photons = \frac{[\langle P \rangle].T.R}{RR.[E]}, \tag{4.2}$$

where $T$ is the transmission coefficient of the UV window (0.922) in front of the cathode, $R$ is the ratio (0.4285) of the beam splitter, and $RR$ is the laser repetition rate of the laser (10 Hz).

### 2. Electron Number Calculation

We recorded the area under the curve of the photoelectron signal on the oscilloscope in order to determine the number of electrons. The area's unit was Vs. So, initially we divided the value by the FCT scale factor, which was 1.25 V/A, and that gave us the amount of the charge (As) carried by the photoelectrons. If we divide this by the charge of one electron, we get the number of electrons in that photoelectron pulse. In the schematic diagram of the electron number calculation (Figure 36), $\langle P \rangle$ is the average power, which is what our laser power meter reads, P(t) is the instantaneous power delivered by the laser, I(t) is the instantaneous current in our test stand, and Q is the amount of charge delivered during one cycle.

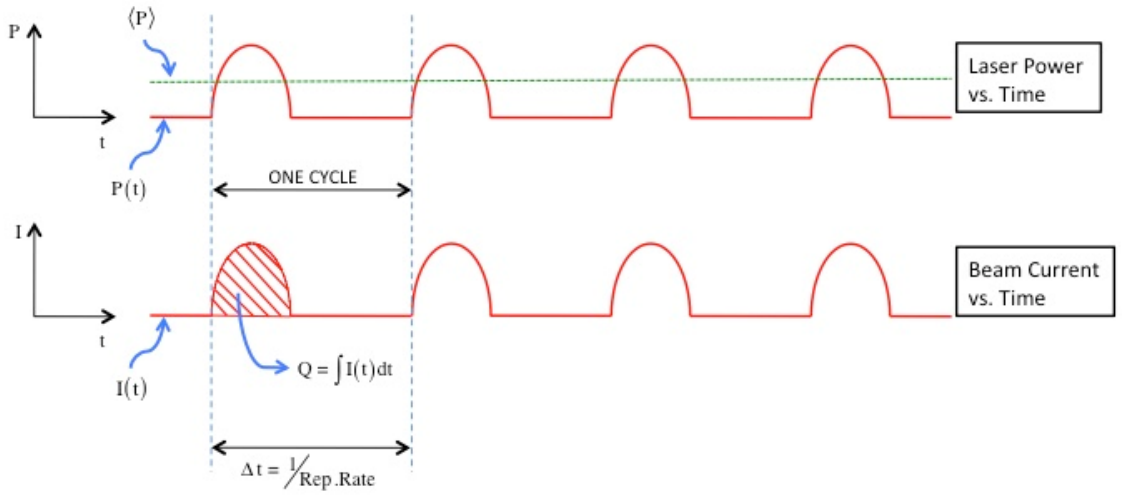


Figure 36. Schematic diagram of electron number calculation.

$$\#electrons = \frac{[Area]}{[FCT\_Factor].e} \tag{4.3}$$

### 3. Quantum Efficiency

To find the QE, we then divide Equation 4.3 by Equation 4.2, which gives

$$QE = \frac{\#electrons}{\#photons} = \frac{Q/\nu}{\langle P \rangle \Delta t / E} \tag{4.4}$$

Because our laser power meter measures the average power $\langle P \rangle$ rather than the instantaneous power $P(t)$, we have effectively chosen to find the QE by comparing the number of photons and electrons delivered in one cycle, rather than by comparing the instantaneous rates of photons reaching the cathode and electrons leaving the cathode (Figure 37).

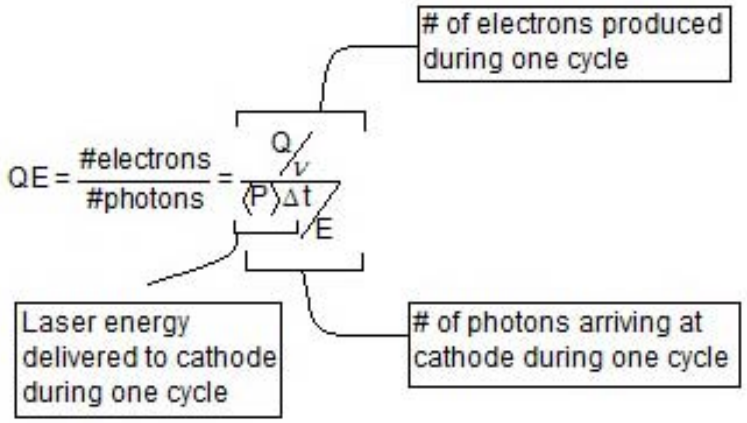


Figure 37. QE per cycle.

### 4. Peak Current Calculation

We used peak current value for defining the SCL regime earlier in this thesis. This value was found from the peak voltage value of the photoelectron pulse on the oscilloscope. First, it was recorded by hand, and second it was divided by the Bergoz FCT factor (1.25 V/A). This value was not directly used

inside the QE calculation because our laser power meter measured average, rather than peak or instantaneous power.

$$Peak\_Current = \frac{[Peak\_Voltage\_Value]}{[FCT\_Factor]} \tag{4.5}$$

## E. ANALYZING THE DATA

We conducted the experiment, gathered the values, and processed the raw data as discussed above. For both samples, we took data at seven different temperature conditions between 85 K and 400 K.

In this section, we present two types of graphs for each sample. Initially, we are presenting graphs composed of the number of photons on the horizontal scale and electrons on the vertical scale. Each graph contains several small circles which represent the data derived from the stand during the experiment, calculated by the equations mentioned earlier. The lower boundary (low-power end) on the data was set by the nonlinear response at the detector (need to keep the power greater than 5 mW on it), and the upper boundary (high-power end) on the data was set by the need to operate below the SCL (less than 4 mW on the cathode).

Three lines were overlaid on each of these graphs. One of them is a linear fit to the data (red); the slope of this line corresponds to the ratio of electrons to photons and, therefore, the QE. The other two lines (blue) are intended to show the boundary of the data. Therefore, the difference between the slopes of these lines and of the linear fit is a measure of the error in our measurement of QE. These boundary lines are only shown in Figures 38 and 46 to demonstrate how the error estimates were determined.

The second type of graph, the eighth for each cathode material, contains the QE values and error estimates for each of the tested cathode temperatures.

## 1. Copper

What follows are seven graphs that show the QE values at different temperature conditions for copper and one summary graph.

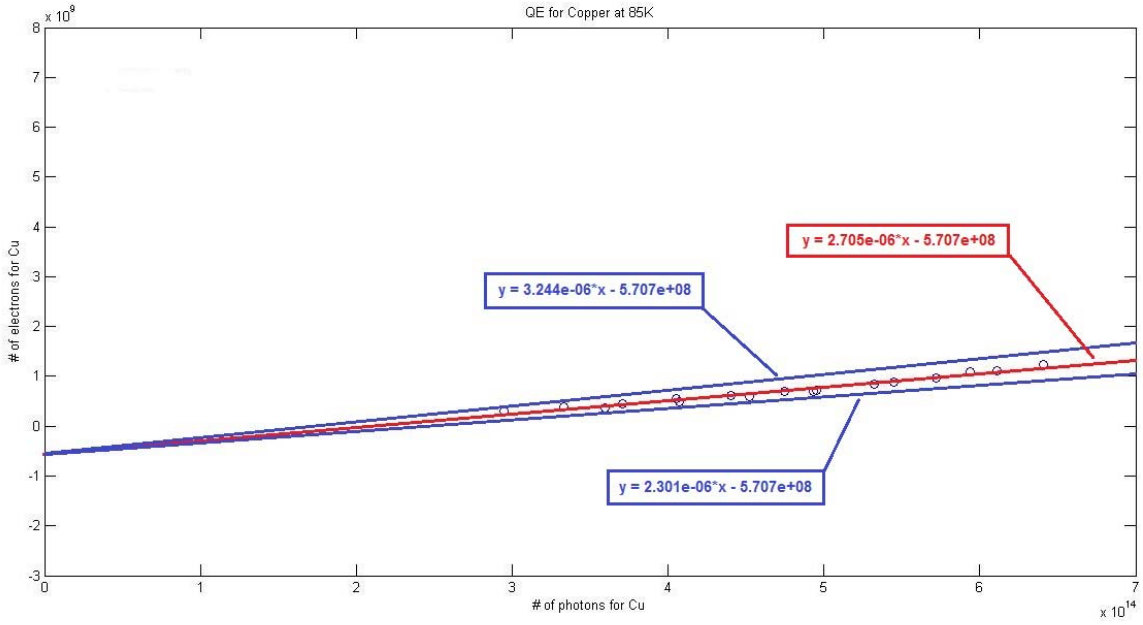


Figure 38. Results for copper at 85 K.

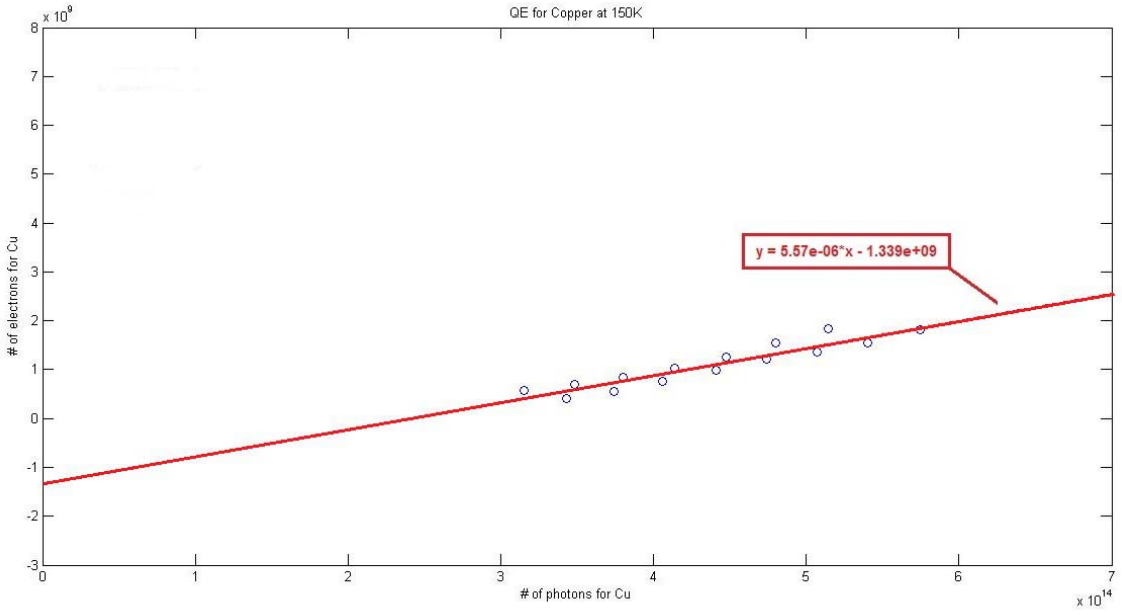


Figure 39. Results for copper at 150 K.

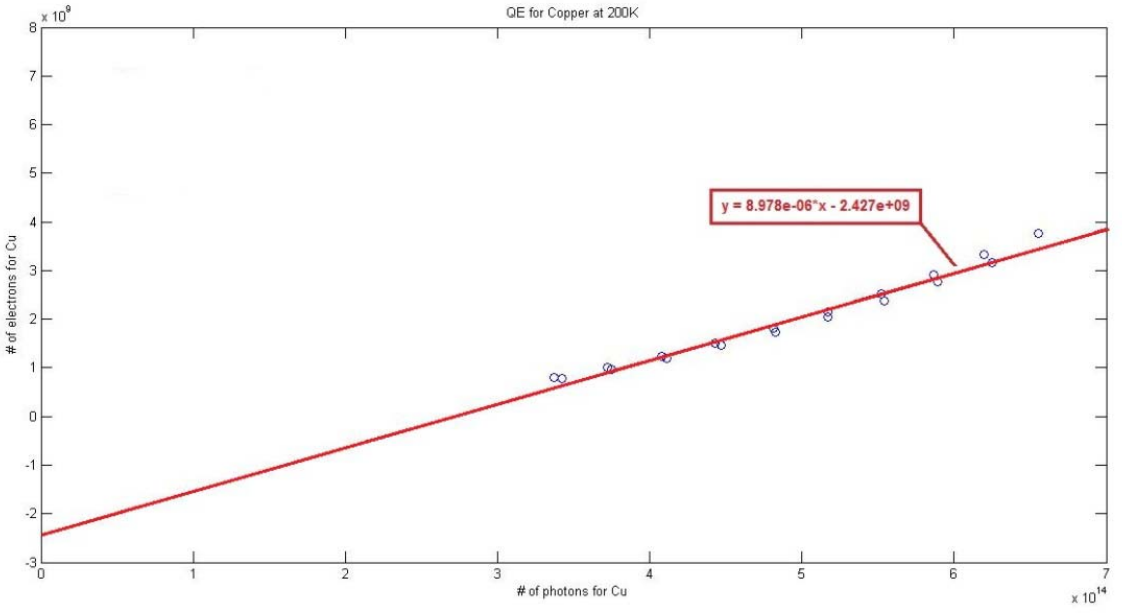


Figure 40. Results for copper at 200 K.

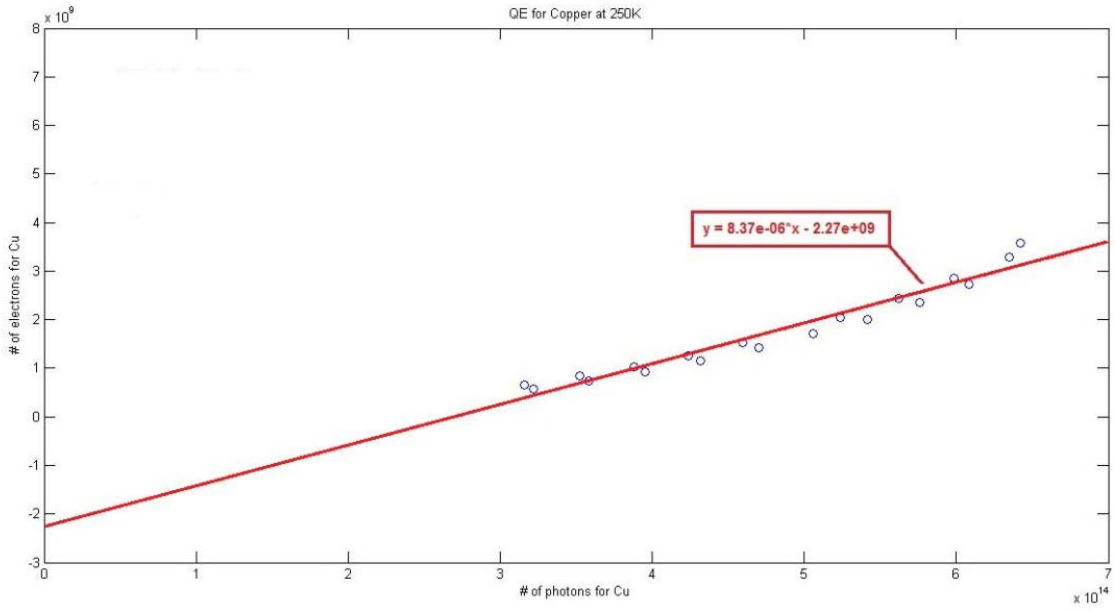


Figure 41. Results for copper at 250 K.

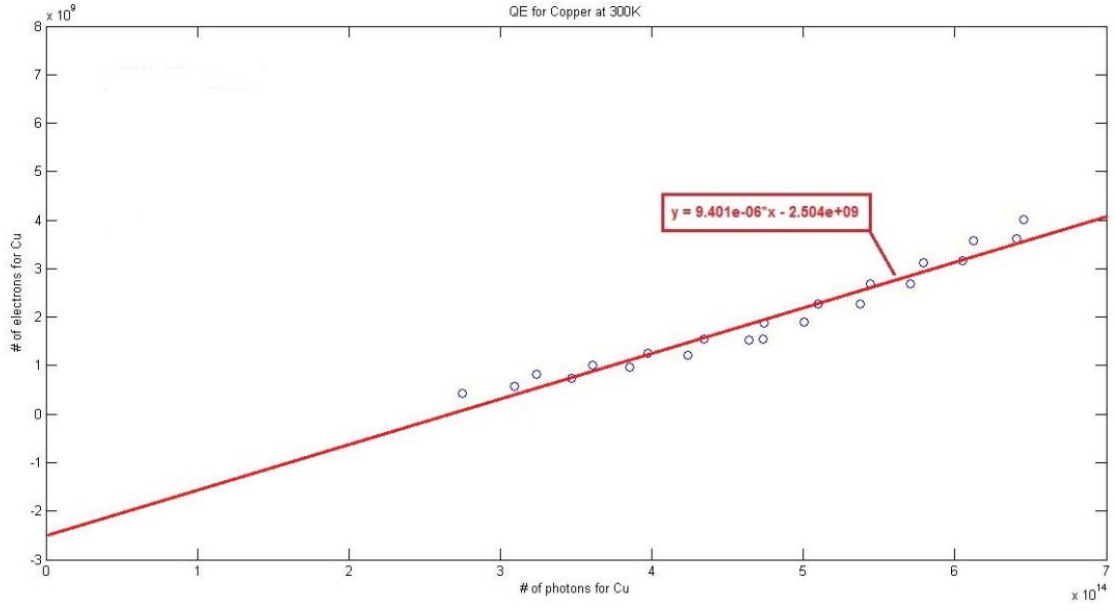


Figure 42. Results for copper at 300 K.

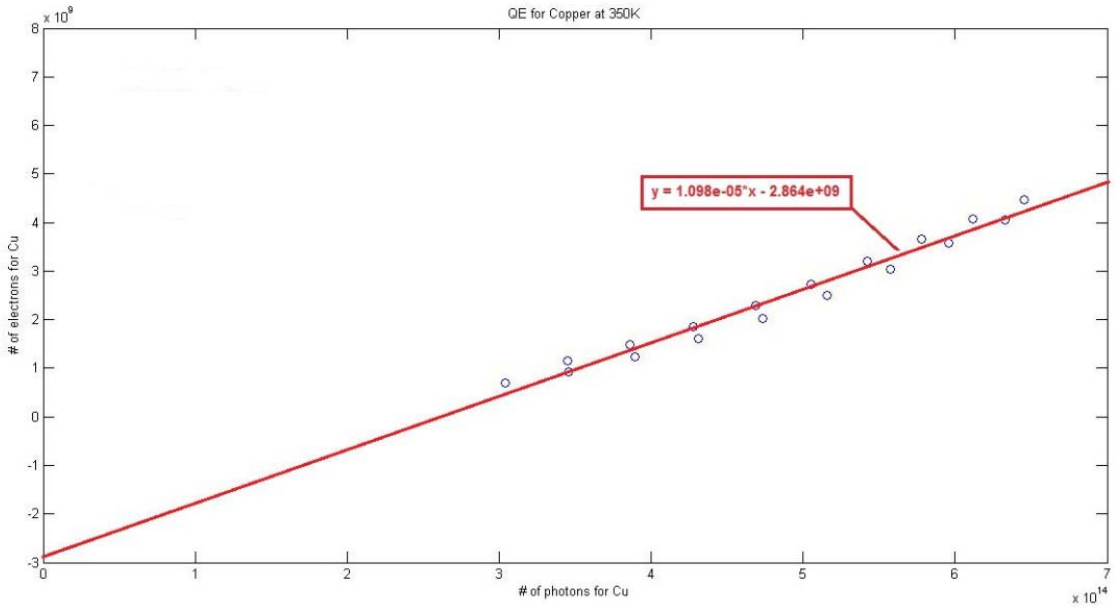


Figure 43. Results for copper at 350 K.

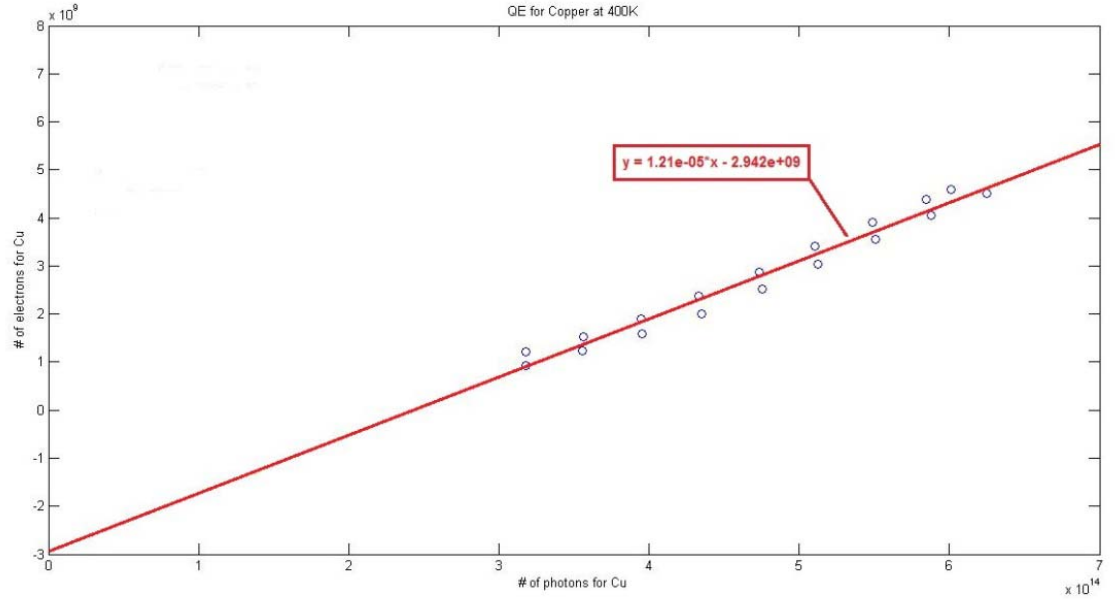


Figure 44. Results for copper at 400 K.

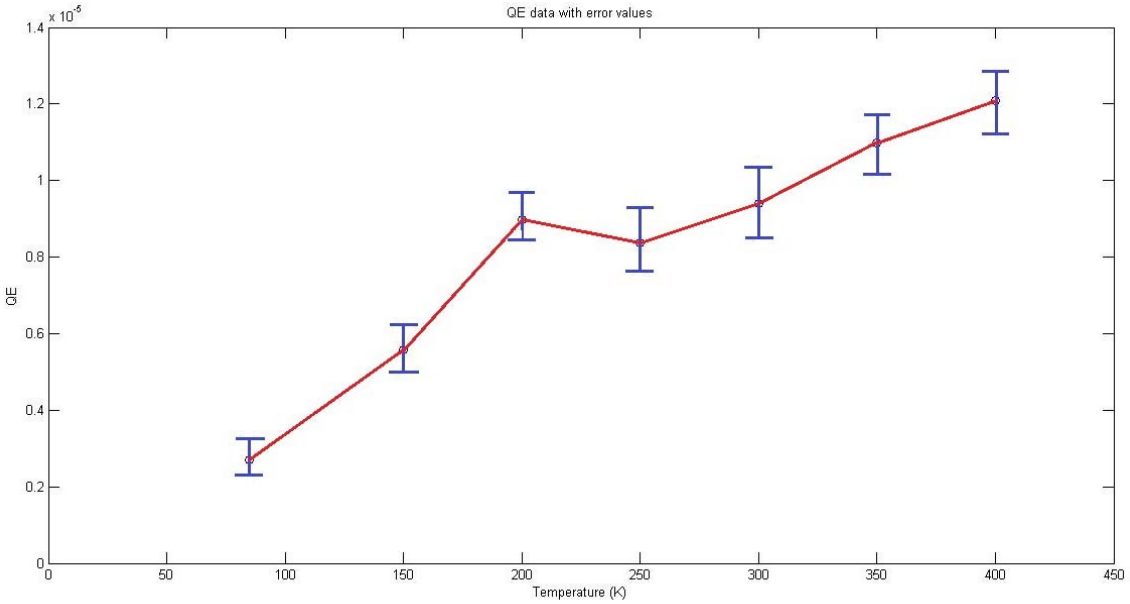


Figure 45. Dependence of QE on temperature for copper.

### 2. Niobium

There are also seven graphs that show the QE values at different temperature conditions for niobium and one summary graph.

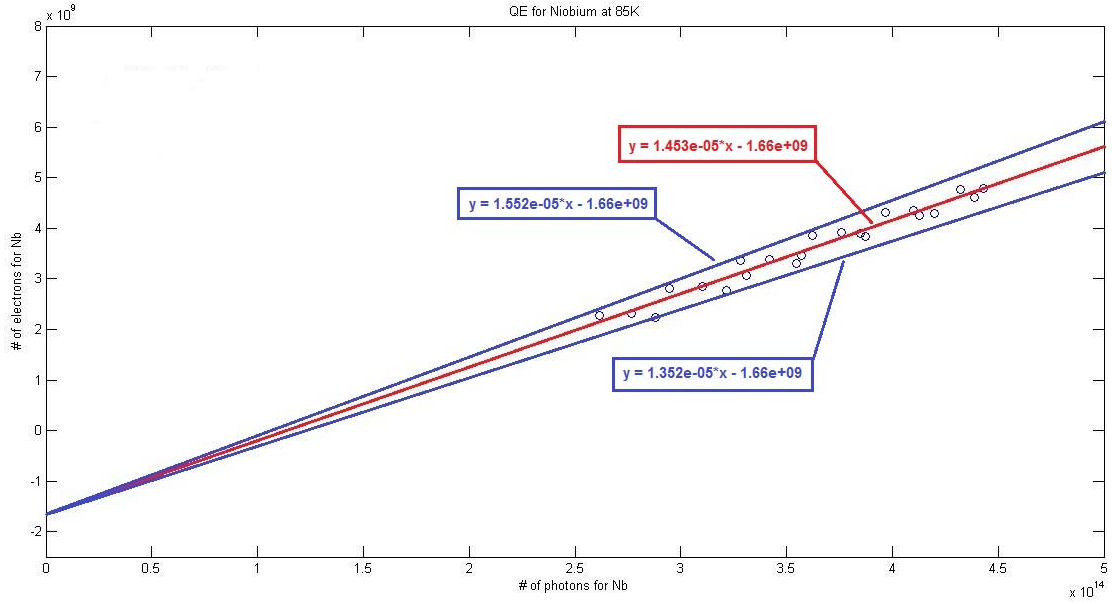


Figure 46. Results for niobium at 85 K.

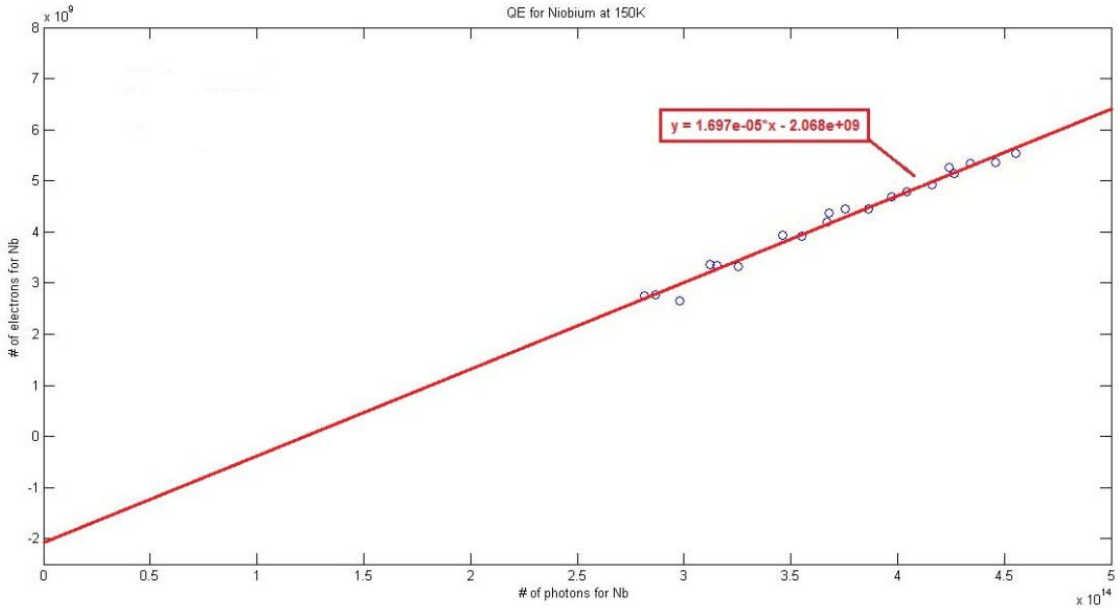


Figure 47. Results for niobium at 150 K.

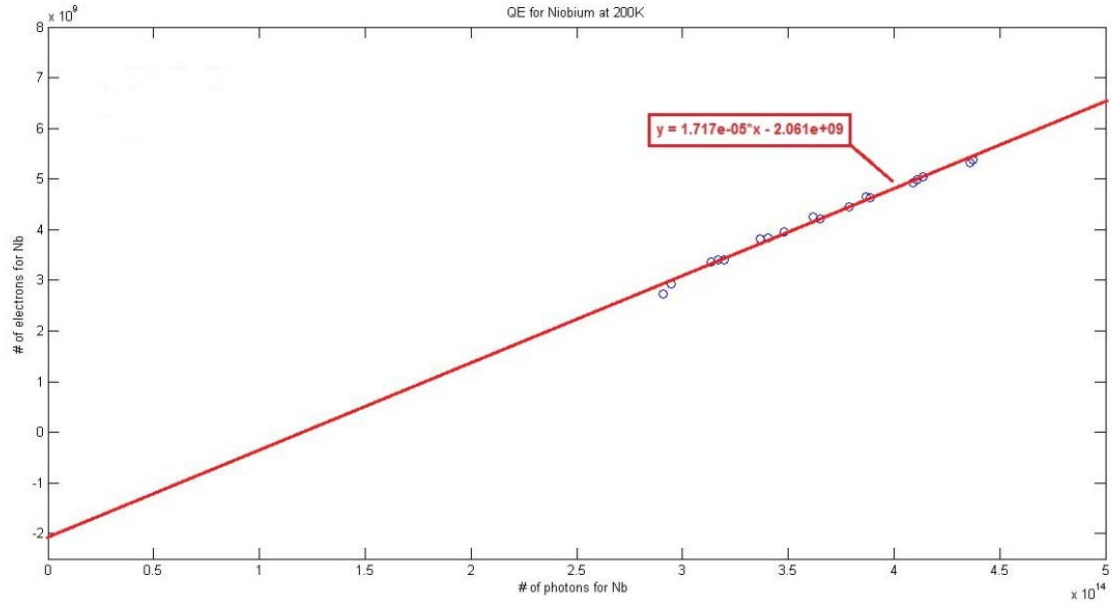


Figure 48. Results for niobium at 200 K.

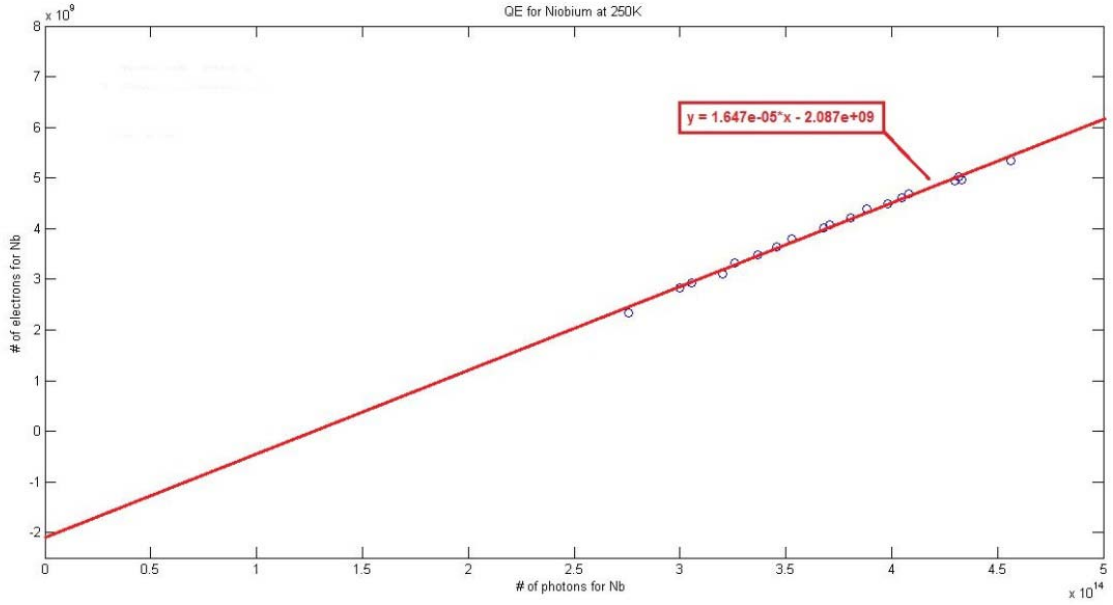


Figure 49. Results for niobium at 250 K.

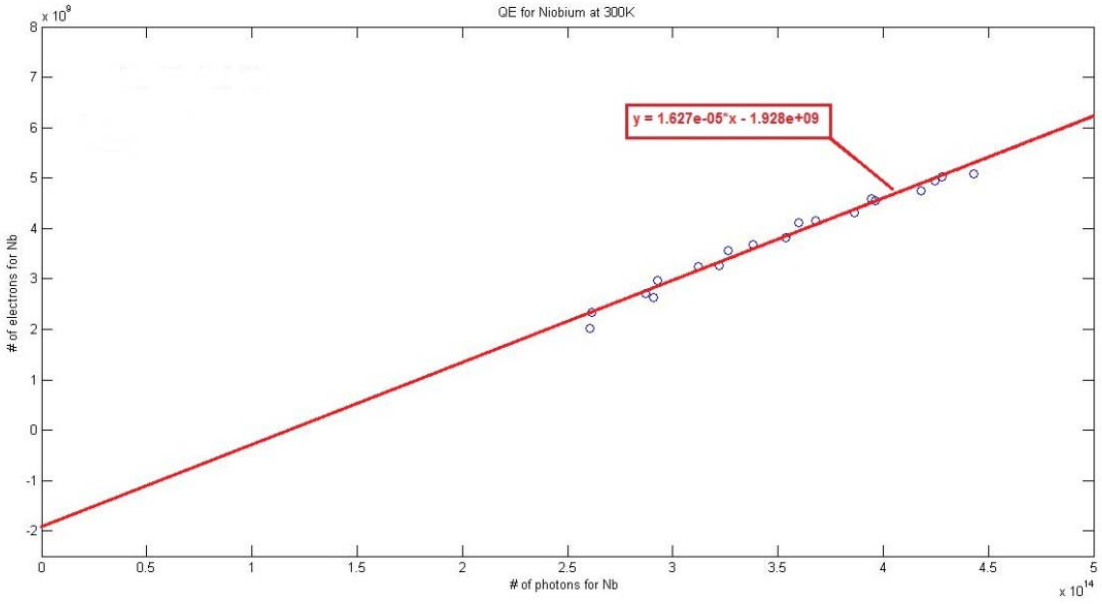


Figure 50. Results for niobium at 300 K.

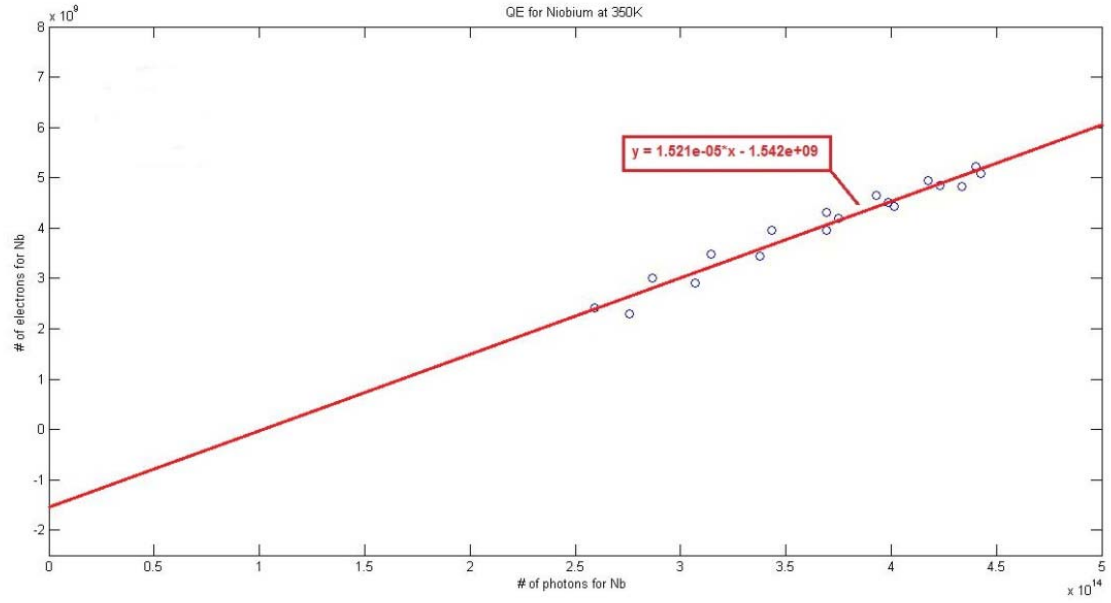


Figure 51. Results for niobium at 350 K.

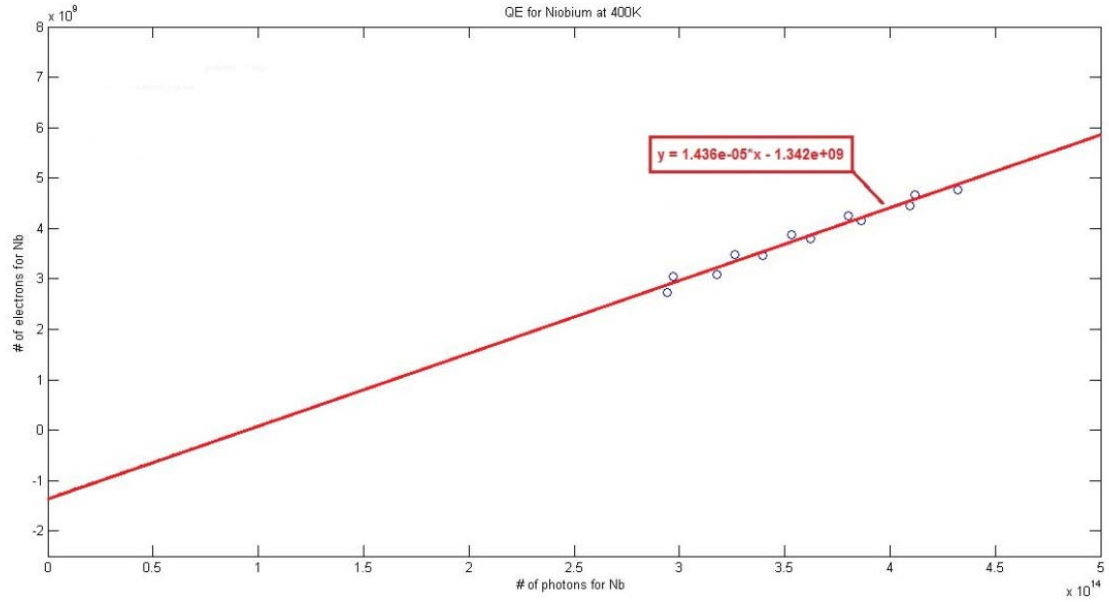


Figure 52. Results for niobium at 400 K.

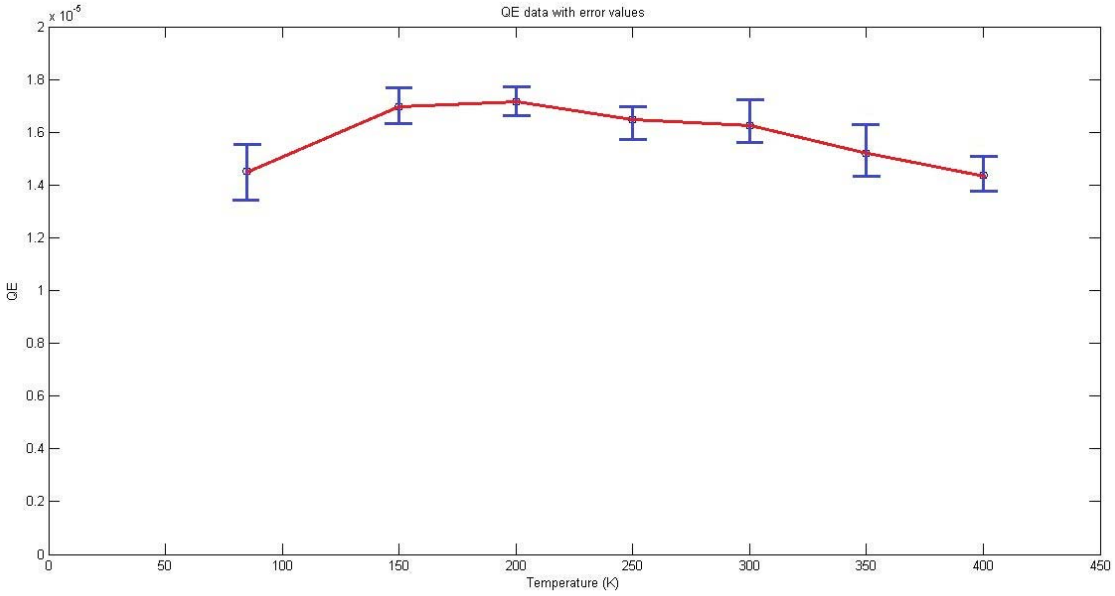


Figure 53. Dependence of QE on temperature for niobium.

# IV. RESULTS AND RECOMMENDATIONS FOR FUTURE WORK

## A. RESULTS FOR COPPER AND NIOBIUM

The primary objective of this project was to see if there was any change in the QE of metal photocathodes as their temperature was varied over a wide range. To answer this simple question, we built our test stand, did experiments, gathered data, and analyzed them as presented in previous chapters.

Figure 45 shows that for copper, there is a clear and statistically significant increase in QE when the temperature was also increased. At 85 K, the QE was $0.27 x 10^{-5}$, while at 400 K, it was $1.2 x 10^{-5}$. This represents an increase in QE by more than a factor of four between these two temperature conditions. Over this range, the trend was almost linear, except for the values at 200 K. The cause of this discrepancy is unknown, but it does not obscure the clear trend evident in the data. When we investigated the vacuum pressure level during the experiments, it remained stable, with the exception of the points at 400 K, indicating that vacuum pressure cannot explain the observed change in QE (Figure 32).

We achieved higher QE values on the niobium cathode than on the copper cathode. However, the observed dependence of QE on temperature for niobium is much weaker than for copper, as shown in Figure 53. The highest QE value was reached at 200 K.

This experiment found *values* of QE for copper and niobium that were generally in line with those reported in the literature (Table 2). Detailed comparisons of QE from one experiment to the next are difficult, because the QE will depend strongly on the sample and testing conditions, which include the cathode surface, vacuum level, and applied fields. But having a single experimental apparatus where the temperature of the cathode can be varied while keeping other influences (such as the cathode surface, applied fields,

testing procedures, and to some degree vacuum pressure) constant, as was done here, helps us more effectively isolate the dependence of QE on temperature.

On the other hand, the difference in the observed *temperature dependence* between the copper results and the niobium results is dramatic and unexplained. The simple theories of photoemission from metals would predict the temperature dependence to be similar for all metals, but that is obviously not the case. There is something going on here that needs further investigation both experimentally and theoretically. The difference could be due to any one of the three steps in the photoemission process: photon absorption, electron transport to the surface and emission over the barrier. It will take a very sophisticated experiment to determine which of these is responsible for the difference.

| Cathode Material | QE | Cathode Temperature | Vacuum Pressure around Cathode | Applied Electric Field/ Voltage |
|---|---|---|---|---|
| **Cu** | **0.27 - 1.2 x 10–$^{5}$** | **Cryogenic (85 K) to 400 K** | **4 - 8 x 10–$^{7}$ Torr** | **10 kV** |
| Cu [32] | 1.4 x 10–$^{4}$ | Room temp. | 10–$^{8}$ - 10–$^{9}$ Torr | 10 kV |
| Cu [33] | 1.0 x 10–$^{4}$ | Room temp. | 10–$^{9}$ Torr | 3.5 MeV |
| Cu [34] | 1.4 x 10–$^{5}$ | Room temp. | 3.7 x 10–$^{7}$ Torr | 550 V |
| Cu [35] | 5.0 x 10–$^{4}$ | Room temp. | 10–$^{7}$ Torr | 130 MV/m |
| **Nb** | **1.4–1.7 x 10–$^{5}$** | **Cryogenic (85 K) to 400 K** | **1–5 x 10–$^{7}$ Torr** | **10 kV** |
| Nb [36] | 2.0 x 10–$^{6}$ | Cryogenic (4 K) | … | … |
| Nb [37] | 5.0 x 10–$^{5}$ | Cryogenic (2 K) | … | … |
| Nb [38] | 1.0x10–$^{7}$<br>5.1x10–$^{5}$ (*) | Room temp. | 5.0 x 10–$^{9}$ Torr | 10 kV |
| Nb [39] | 7.4x10–$^{7}$<br>6.5x10–$^{5}$ (*) | Room temp. | 5.0 x 10–$^{9}$ Torr | 10 kV |
| Nb [40] | 1.2 x 10–$^{5}$ | Room temp. | … | 1 kV |
| Nb [12] | 1.0 – 2.0 x 10–$^{6}$ | Cryogenic (4.2 K) | 10–$^{8}$ Torr | 29 MV/m |

Table 2. Quantum efficiency for copper and niobium illuminated with 266 nm light.

Note that in Table 2, bold fond indicates results obtained in this thesis. Asterisks (*) denote values achieved after surface cleaning.

## B. RECOMMENDATIONS FOR FUTURE WORK

As previously stated, while we were doing experiments, we utilized two pumps to try to maintain a constant vacuum environment inside the vacuum chamber. However, this situation could not be provided at all times. Whenever we increased the cathode temperature from a low level to a higher level, we observed that the vacuum level started to increase, as well. Although, we waited long enough after changing the cathode temperature to allow the system to reach its previous vacuum level, we could not achieve the UHV vacuum condition, especially for high temperatures, such as 300 K, 350 K, and 400 K. In the future more powerful vacuum pumps can be used to supply a more stable vacuum environment around the cathode during the experiment process, and the system should be baked out at high temperatures to remove all adsorbed gases.

There is room for improvement in other areas, also. If the high voltage could be raised from 10 kV to a much higher value, such as 100 kV, the space charge limited regime could be avoided more easily, and higher laser powers could be used. This requires a more advanced design of the cathode-anode system, though, and would also require shielding and safety procedures to protect experimenters from ionizing radiation.

The laser power detector and meter were not the best ones for this experiment, and the power meter was working at the very low limit of its sensitivity. The laser light was only present for 5 ns every 100 ms, but the detector was measuring power during the whole interval. This caused uncertainty in the measurements. A detector that could measure the energy of each pulse during the short pulse time instead of integrating the power over all time would be a better choice and should give better and more accurate results

Finally, a potential source of error here is the degree to which the surface of these metals had been oxidized or contaminated. A potential way to deal with this is to clean the surface during testing, for example using bombardment by Argon ions.

# LIST OF REFERENCES


[1] J. Cook, “High-energy laser weapons since the early 1960s,” *Optical Eng.,* vol. 52, no. 2, pp. 021007–021007, 2013.

[2] E. T. Gerry and D. A. Leonard, “Measurement of 10.6-μ $CO_2$ laser transition probability and optical broadening cross sections,” *Appl. Physics Letters,* vol. 8, no. 9, pp. 227–229, 1966.

[3] J. R. Albertine, “Recent high-energy laser system tests using the MIRACL/SLBD,” in *OE/LASE ‘93: Optics, Electro-Optics, & Laser Applications in Science& Engineering*, pp. 229–239 Int. Soc. for Optics and Photonics, vol. 1871, 1993.

[4] “Laser,” [Online], Available: http://en.wikipedia.org/wiki/Laser [accessed 14 Dec 2012].

[5] W B. Colson and A. M. Sessler, “Free electron lasers,” *Annu. Rev. of Nucl. and Particle Sci.,* vol. 35, no. 1, pp. 25–54, 1985.

[6] J.R. Harris, (2013, Feb. 25). E-mail message to author.

[7] J. R. Cook and J. R. Albertine, “The navy’s high energy laser weapon system,” in *Proc.-Spie The Int. Soc. for Optical Eng.*, pp. 264–271,1997.

[8] “ONR Free Electron Laser,” [Online], Available: www.onr.navy.mil/en/Media-Center/Fact-Sheets/Free-Electron-Laser.aspx [accessed 14 Dec 2012].

[9] W. B. Colson, “Introduction to the free electron laser,” PH 4858, class notes, Naval Postgraduate School, Monterey, CA, 2012.

[10] “RI Research Instrument GmbH,” [Online], Available: www.research-instruments.de/frontend/products-european-xfel [accessed 14 Jun 2013].

[11] S. P. Niles, W. B. Colson, K. L. Ferguson, J. R. Harris, J. W. Lewellen, B. Rusnak, R. Swent, “NPS prototype superconducting 500 MHz quarter-wave gun update,” in *Proc. of the 20l0 FEL Conf., Malmö*, Sweden, 2010, pp. 457–460.

[12] J. R. Harris, K. L. Ferguson, J. W. Lewellen, S. P. Niles, B. Rusnak, R. L. Swent, W. B. Colson, T. I. Smith, C. H. Boulware, T. L. Grimm, P. R. Cunningham, M. S. Curtin, D. C. Miccolis, D. J. Sox, W. S. Graves, “Design and operation of a superconducting quarter-wave electron gun,” *Phys. Rev. Special Topics-Accelerators and Beams,* vol. 14, no. 5, p. 053501, 2011.

[13] A.I. Yilmaz, “Development and experimental operation of a flashboard plasma cathode test stand,” M.S. thesis, Applied Physics Dept., Naval Postgraduate School, Monterey, CA,, 2012.

[14] J.Z. Buchwald, *The Creation of Scientific Effects: Heinrich Hertz and Electric Waves*. Chicago, IL: Univ. of Chicago Press, 1994.

[15] A. Einstein, *Sidelights on relativity,* Dover, Mineola, New York, 1983.

[16] A.H. Sommer, *Photoemissive Materials*. New York: John Wiley & Sons, 1968, pp. 21–26.

[17] X.J. Wang, M. Babzien, R. Malone, Z. Wu, “Mg cathode and its thermal emittance,” *Proc. of LINAC 2002*, Gyeongju, Korea, pp. 142–144, 2002.

[18] D. H. Dowell., I. Bazarov, B. Dunham, K. Harkay, C. Hernandez-Garcia, R. Legg, H. Padmore, T. Rao, J. Smedley, and W. Wan, “Cathode R&D for future light sources,” *Nuclear Instruments and Methods in Physics Research Section A: Accelerators, Spectrometers, Detectors and Associated Equipment,* vol. 622, no. 3, pp. 685–697, 2010.

[19] K. L. Jensen and E. J. Montgomery, “Photoemission theory and the development of high performance photocathodes,” *J. of Computational and Theoretical Nanosci.,* vol. 6, no. 8, pp. 1754–1769, 2009.

[20] K. L. Jensen, “Electron emission physics,” *Advances in Imaging and Electron Physics,* vol.149, pp. 147–279, 2007.

[21] E. J. Montgomery, D. W. Feldman, P. G. O’Shea, J. C. Jimenez, J. R. Harris, K. L. Jensen, “Cesium emission in dispenser photocathodes,” *Proc. of the 20l0 FEL Conf.,* pp. 422–424, 2010.

[22] J. C. Jimenez, . “A systematic cathode study - Activation of a thermionic cathode, and measuring cesium evaporation from a dispenser photocathode.” M.S. thesis, Applied Physics Dept., Naval Postgraduate School, Monterey, CA, 2010.

[23] T. Maruyama, R. Prepost, E. L. Garwin, C. K. Sinclair, B. Dunham and S. Kalem, “Enhanced electron spin polarization in photoemission from thin GaAs,” *Appl. Physics Lett.,* vol. 55, no. 16, pp. 1686–1688, 1989.

[24] C. K. Sinclair, “Recent advances in polarized electron sources,” *Proc. of the IEEE Particle Accelerator Conf.*, vol. 1, pp. 65–69, 1999.

[25] R. J. Umstattd., C. A. Schlise, and F. Wang. “Gas evolution during operation of a CsI-coated carbon fiber cathode in a closed vacuum system,” *Plasma Science*, *IEEE Trans.*, vol. 33, no. 2, pp.901–910, 2005.

[26] K. L. Jensen, N. A. Moody, D. W. Feldman, E. J. Montgomery, and P. G. O'Shea. "Photoemission from metals and cesiated surfaces." *J. of Appl. Physics,* vol. 102, no. 7, p. 074902–074902, 2007.

[27] K. L. Jensen, P. G. O'Shea, D. W. Feldman, and N. A. Moody. "Theoretical model of the intrinsic emittance of a photocathode," *Appl. Physics Lett.,* vol. 89, no. 22,pp. 224103–224103, 2006.

[28] N. A. Moody, Kevin L. Jensen, Donald W. Feldman, Eric J. Montgomery, and Patrick G. OShea. "Factors affecting performance of dispenser photocathodes," *J. of Appl. Physics,* vol.102, no. 10, pp. 104901–104901, 2007.

[29] J. G. Neumann, J. R. Harris, B. Quinn and P. G. O'Shea, "Production of photoemission-modulated beams in a thermionic electron gun," *Rev.of Sci. Instrum.,* vol. 76, no. 3, pp. 033303–033303, 2005.

[30] A. B. Baxter, "Cathode stalk cooling system for the MK1 quarterwave gun." M.S. thesis, Applied Physics Dept., Naval Postgraduate School, Monterey, CA, 2012.

[31] J.R. Harris. (2013, May 20). E-mail message to author.

[32] T. Srinivasan-Rao, J. Fischer, and T. Tsang, "Photoemission studies on metals using picosecond ultraviolet laser pulses," *J. of Appl. Physics*, vol. 69, no. 5, pp. 3291–3296,1991.

[33] P. Davis, G. Hairapetian, C. Clayton, C. Joshi, S. Hartman, S. Park, C. Pellegrini, and J. Rosenzweig, "Quantum efficiency measurements of a copper photocathode in an RF electron gun," *Proc. of the IEEE Particle Accelerator Conference*, pp. 2976–2978,1993.

[34] E. B. Sozer, Chunqi Jiang, Martin A. Gundersen, and R. J. Umstattd, "Quantum efficiency measurements of photocathode candidates for back-lighted thyratrons." *Dielectrics and Electrical Insulation, IEEE Trans*. vol. 16, no. 4, pp. 993–998, 2009.

[35] X. J. Wang, M. Babzien, K. Batchelor, I. Ben-Zvi, R. Malone, I. Pogorelsky, X. Qui, J. Sheehan, J. Sharitka, and T. Srinivasan-Rao, "Experimental characterization of the high-brightness electron photoinjector," *Nuclear Instruments and Methods in Physics Research Section A: Accelerators, Spectrometers, Detectors and Associated Equipment*, vol. 375, no. 1, pp. 82–86, 1996.

[36] T. Srinivasan-Rao, I. Ben-Zvi, A. Burrill, H. Hahn, D. Kayran, Y. Zhao, and M. Cole. “Photoemission studies on BNL/AES/JLAB all niobium, superconducting RF injector.” In Proc. IEEE of the Particle Accelerator Conference, pp. 2556–2558, 2005.

[37] T. Srinivasan-Rao, I. Ben-Zvi, A. Burrill, G. Citver, A. Hershcovitch, D. Pate, A. Reuter et al., “Design, construction and status of all niobium superconducting photoinjector at BNL,” *Proc. IEEE of the Particle Accel. Conf*, vol. 1, pp. 92–94, 2003.

[38] Q. Zhao, Triveni Srinivasan-Rao, and Mike Cole. “Tests of niobium cathode for the superconducting radio frequency gun,” *Proc. IEEE of the Particle Accelerator Conference,* vol. 3, pp. 2047–2049, 2003.

[39] J. Smedley, T. Rao, and Q. Zhao. “Photoemission studies on niobium for superconducting photo injectors,” *J. of Appl. Physics*, vol. 98, no. 4,pp. 043111–043111, 2005.

[40] J. Smedley, Triveni Rao, B. N. L. John Warren, and D. E. S. Y. Jacek Sekutowicz, “Photoemission Properties of Lead.” *Proc. European Part. Accel. Conf.*, p. 1126, 2004.

# INITIAL DISTRIBUTION LIST

1. Defense Technical Information Center
   Ft. Belvoir, Virginia

2. Dudley Knox Library
   Naval Postgraduate School
   Monterey, California